Mature oligodendrocytes bordering lesions limit demyelination and favor myelin repair via heparan sulphate production

24 Hills Road, **P** 01223 855346
Cambridge **W** elifesciences.org
CB2 1JP **T** @elife_sciences

FOR PEER REVIEW - CONFIDENTIAL

Mature oligodendrocytes bordering lesions limit demyelination and favor myelin repair via heparan sulphate production

Tracking no: 08-09-2019-RA-eLife-51735R1

Impact statement: Heparan sulfate synthesis by mature oligodendrocytes creates a protective and permissive environment controling microglia and oligodendrocyte progenitors reactivation during remyelination.

Competing interests: No competing interests declared

Author contributions:
Magali Macchi: Conceptualization; Formal analysis; Investigation; Methodology; Writing - original draft Karine Magalon: Conceptualization; Formal analysis; Investigation; Methodology; Writing - review and editing Céline Zimmer: Conceptualization; Formal analysis; Writing - original draft Elista Peeva: Formal analysis Bilal El Waly: Formal analysis Béatrice Brousse: Formal analysis Sarah Jaekel: Formal analysis Kay Grobe: Formal analysis; Validation; Writing - original draft Friedemann Kiefer: Resources Anna Williams: Formal analysis; Supervision; Investigation; Methodology; Writing - original draft; Writing - review and editing Myriam Cayre: Conceptualization; Formal analysis; Supervision; Validation; Investigation; Methodology; Writing - original draft; Writing - review and editing Pascale Durbec: Conceptualization; Supervision; Funding acquisition; Validation; Methodology; Project administration

Funding:
Centre National de la Recherche Scientifique (CNRS): Pascale Durbec, financial support; Aix-Marseille Université (AMU): Pascale Durbec, Graduate student Fellowship and financial support; Fondation pour la Recherche Médicale (FRM): Pascale Durbec, DEQ20140329501; Agence Nationale de la Recherche (ANR): Pascale Durbec, France-bioimaging/PICSL infrastructure ANR-10-INSB-04-01; Agence Nationale de la Recherche (ANR): Pascale Durbec, ANR-15-CE16-0014-01; AM*DEX NeuroMarseille Institute: Pascale Durbec, AMX-19-IET-004 The funders had no role in study design, data collection and interpretation, or the decision to submit the work for publication.

Data Availability:
All data generated or analysed during this study are included in the manuscript and supporting files.
N/A

Ethics:
Human Subjects: Yes Ethics Statement: Human postmortem unfixed frozen tissues were obtained from the UK Multiple Sclerosis Tissue Bank via a UK prospective donor scheme with full ethical approval (MREC/02/2/39). Clinical Trial: No Animal Subjects: Yes Ethics Statement: All experimental and surgical protocols were performed following the guidelines established by the French Ministry of Agriculture (Animal Rights Division). The architecture and functioning rules of our animal house, as well as our experimental procedures have been approved by the 'Direction Départementale des Services Vétérinaires' and the ethic committee (ID numbers F1305521 and 2016071112151400 for animal house and research project,

Information for reviewers (full submissions):

eLife aims to publish work of the highest scientific standards and importance in all areas of the life and biomedical sciences, from the most basic and theoretical work through to translational, applied and clinical research. Articles must be methodologically and scientifically rigorous, ethically conducted, and objectively presented according to the appropriate community standards.

You will be asked for a general assessment and a summary of any major concerns (ideally in fewer than 500 words), as well as a list of any minor comments (optional). You will also have the opportunity to comment on the statistical rigour of the work (optional).

In your general assessment, please articulate what is exciting and whether the work represents a significant contribution. Please note our guidelines about requests for additional work:

1. We will only request new work, such as experiments, analyses, or data collection, if the new data are essential to support the major conclusions. The authors must be able to do any new work in a reasonable time frame (additional work should be conducted and written up within two months); otherwise, we will usually reject the manuscript.
2. Any requests for new work must fall within the scope of the current submission and the technical expertise of the authors.

Our goal is to make peer review constructive and collaborative: after the reviews have been submitted independently, there is an online

discussion between the reviewers in which each reviewer will see the identity of the other reviewers.

Mature oligodendrocytes bordering lesions limit demyelination and favor myelin repair via heparan sulphate production

Magali Macchi[1#], Karine Magalon[1#], Céline Zimmer[1], Elitsa Peeva[2], Bilal El Waly[1], Béatrice Brousse[1], Sarah Jaekel[2], Kay Grobe[3], Friedemann Kiefer[4], Anna Williams[2], Myriam Cayre[1] and Pascale Durbec [1]*

[1]Aix Marseille Univ, CNRS, IBDM, Marseille, France

[2]MRC Centre for Regenerative Medicine, Multiple Sclerosis Society Centre for Translational Research, University of Edinburgh, Edinburgh, UK.

[3]Institute of Physiological Chemistry and Pathobiochemistry and Cells-in-Motion Cluster of Excellence (EXC1003-CiM), University of Münster, Münster, Germany.

[4]Max Planck Institute for Molecular Biomedicine. Münster Germany.

#; These authors contributed equally

*Corresponding author: Pascale Durbec, PhD.
Aix Marseille Univ, CNRS, IBDM, Marseille, France. Case 907, Parc Scientifique de Luminy 13288 MARSEILLE Cedex 09. France.
Telephone: +33-491 269 746.
Fax:+33-491 269 316.
E-mail: pascale.durbec@univ-amu.fr

Number of pages: 42

Number of figures: 7 and 6 supplementary

Keywords: Demyelination, Heparan sulfate, N-deacetylase-N-sulfotransferase 1, Oligodendrocyte lineage cells, Multiple Sclerosis

Abstract

Myelin destruction is followed by resident glia activation and mobilization of endogenous progenitors (OPC) which participate in myelin repair. Here we show that in response to demyelination, mature oligodendrocytes (OLG) bordering the lesion express Ndst1, a key enzyme for heparan sulfates (HS) synthesis. Ndst1+ OLG form a belt that demarcates lesioned from intact white matter. Mice with selective inactivation of Ndst1 in the OLG lineage display increased lesion size, sustained microglia and OPC reactivity. HS production around the lesion allows Sonic hedgehog (Shh) binding and favors the local enrichment of this morphogen involved in myelin regeneration. In MS patients, Ndst1 is also found overexpressed in oligodendroglia and the number of Ndst1-expressing oligodendroglia is inversely correlated with lesion size and positively correlated with remyelination potential. Our study suggests that mature OLG surrounding demyelinated lesions are not passive witnesses but contribute to protection and regeneration by producing HS.

INTRODUCTION

In multiple sclerosis (MS), OLG are the target of inflammatory and immune attacks and their death results in multiple focal demyelinated lesions in the CNS. Myelin loss remains in defined areas, rather than expanding to involve all of the white matter, and the mechanism by which demyelinated lesions stop expanding is not understood. Some of these lesions may stop expanding as inflammation is controlled and lesions are remyelinated. Remyelination involves OPC recruitment to the lesion, differentiation into myelin forming cells and remyelination of denuded axons, and the success of this depends on environmental context, including secreted factors from neighboring cells [1, 2]. This repair process, which occurs spontaneously in MS patients, is highly variable between patients and between lesions [2]. Regenerative failure is mainly attributed to defects in OPC recruitment towards the demyelinated areas [3] and/or to their incapacity to differentiate into myelinating OLG at the lesion site [1, 4-6].

Multiple factors are involved in this regenerative process including those produced by reactive astrocytes or microglia and macrophages [7]. These contribute to myelin destruction, but also to myelin debris removal and beneficial effects by secreting factors that directly or indirectly support remyelination [8-13]. Interestingly oligodendrocyte lineage cells also produce factors that modulate remyelination, such as the morphogen shh which is produced by OLG and OPC at the onset of demyelination in lysophosphatidyl choline (LPC)-induced lesions [14]. In this context, blocking Shh activity induces an increase in lesion size and a block in OPC proliferation and differentiation, and conversely Shh overexpression leads to the attenuation of the lesion extent and promotes oligodendrogenesis [14]. Identifying such actors involved in myelin damage and remyelination is needed for the design of future protective and regenerative therapies.

The presence of a multitude of signals regulating specific steps of remyelination raises the hypothesis that key factors may be necessary to integrate all these cues. One of these key factors may be HS proteoglycans (HSPG), as there is now compelling evidence that HSPGs play a critical role in regulating spatiotemporal coordination of signals in the extracellular microenvironment of many tissues during brain development and in adulthood [15]. HS chains consist of linear repeated disaccharide units of N-acetyl glucosamine and glucuronic acid which are synthesized on proteoglycan core proteins. Ndst enzymes perform the first step of these sugar modifications thus specifying the functional properties of HSPGs [16-18]. Among the four known Ndst enzymes, Ndst1 appears as the key enzyme for addition of N-sulfated motifs to HS chains in brain during development, as shown by limited functional redundancy mediated by other Ndst enzymes (2-4) in *Ndst1* KO mice [19, 20]. During development, HS proteoglycans provide an important signaling scaffold allowing spatial concentration or trapping of numerous molecules such as morphogens and growth factors [21] and the control of receptor activity [21-24]. Following CNS injury, HSPGs are known to play a pivotal role in post-lesional plasticity and regeneration [25] [26]. Some HS proteoglycans are over-expressed by reactive astrocytes in injured mouse brain and provide positive [25] or negative [26] environmental support for axon regenerative responses. In vitro, HS proteoglycans can prevent OLG differentiation, maintaining OPC in an immature proliferative phenotype by acting as a FGF-2 co-receptor [27, 28]. Therefore, we hypothesized that HS proteoglycans play an organizing role in controlling myelin damage and repair.

Here we show that mature OLG bordering a demyelinated lesion limit lesion extension and influence OPC mobilization via HS production. Using a model of acute focal demyelination of the corpus callosum in mice, we show that *Ndst1* expression is induced in OLG around the lesion throughout the phases of demyelination and remyelination. *Ndst1* expression and subsequent HS accumulation mostly accumulate at the margin of the lesion,

delimiting the lesion from the intact corpus callosum during demyelination. To evaluate the relevance of Ndst1 induction for lesion formation and repair, we exposed genetically modified mice with selective deletion of *Ndst1* in oligodendroglia to focal demyelination of the corpus callosum. Lack of Ndst1 in OLG resulted in an increased lesion size, and a sustained OPC and microglia/macrophage activation at the early stage of remyelination. HS enrichment correlates with and is necessary for the binding around the lesion site of the morphogen Shh, suggesting that Ndst1 expression and HS secretion by OLG enhances Shh signaling after demyelination, thus favoring remyelination [14, 29]. Furthermore, NDST1 expression in OLG was also increased in human postmortem tissues from multiple sclerosis patients. This increased density of NDST1+ OLG in lesions was inversely correlated with the size of the lesion and positively correlated with remyelination.

RESULTS

Demyelination triggers *Ndst1* up-regulation by OLG and creates a transient N-sulfated belt around the lesion

To identify candidates that could regulate interactions between progenitors and the injured environment, a microarray analysis was performed to compare gene expression in purified oligodendroglia from adult healthy and demyelinated animals [30]. One of the most robustly and significantly up-regulated genes after demyelination was *Ndst1*, a key enzyme of HS proteoglycan synthesis (fold increase of 48.9 and 14.0 in two different trials; $p \leq 0.001$; microarray data are available at GEO with accession number GSE47486). This up-regulation of *Ndst1* was confirmed *in vivo* at 21 days in mice exposed to EAE by in situ hybridization combined with Olig2 labeling, a pan OLG marker. While *Ndst1* was not detected in the corpus callosum of control brains (Figure 1-figure supplement 1A), it was highly expressed

by the Olig2+ population after EAE in the corpus callosum (Figure 1-figure supplement 1B-C) in close proximity to lesion sites (Figure 1-figure supplement 1C).

To characterize the up-regulation of *Ndst1* after demyelination, we used LPC to trigger focal demyelination lesions in the mouse corpus callosum (Figure 1A). In this model, demyelination is not T cell driven, and demyelination and remyelination proceed in a stereotypic sequence: demyelination occurs within few days, endogenous progenitor mobilization peaks at 8 dpi and is followed by OPC differentiation [8]. Production of new myelin is then observed after 2 weeks. Demyelination of the corpus callosum is clearly visible after LPC injection in a reporter mouse where myelin fluoresces green (*plp-GFP*) [31, 32] by the total loss of GFP signal around the injection site (Figure 1-figure supplement 2). The lesion is also characterized by a strong increase in cell density (due to glia proliferation and to microglia/macrophage infiltration) observed by Hoechst staining (Figure 1-figure supplement 2) that strictly coincides with loss of GFP fluorescence.

We first evaluated *Ndst1* expression levels by performing RT-qPCR analysis using the corpus callosum of healthy or demyelinated mice on the ipsi- and contralateral sides to the LPC injection, 8 days post injection (dpi). We quantified a mean 41% increase in the *Ndst1* expression level in the demyelinated corpus callosum compared to healthy corpus callosum (Figure 1B; p=0.05). *Ndst1* transcripts were found up-regulated in demyelinated corpus callosum by in situ hybridization at 5 dpi during demyelination (Figure 1C-F), 8 dpi (Figure 1G), and 14 dpi (Figure 1H). At days 5 and 8 dpi, *Ndst1* expressing cells delimited a belt around the lesion site. Weak staining was observed distal to the lesion, in the contralateral side of the corpus callosum and at the core of the lesion (Figure 1C-D). Thus, the induction of demyelination in the corpus callosum triggers *Ndst1* up-regulation, and this change is sustained throughout the phases of demyelination and remyelination.

Since Ndst1 catalyzes a mandatory step in the synthesis of HS chains, its expression is likely to reflect the distribution of HS. We thus examined the outcome of Ndst1 activity by analyzing the distribution of N-sulfated motifs after demyelination. To do so, we used the anti-HS antibody 10E4 [19, 33], which exclusively detects the N-sulfated motifs produced by Ndst1 activity [20]. While no staining was detected in the contralateral corpus callosum (Figure 2A), N-sulfated HS positive puncta formed a belt around the demyelination lesion (Figure 2B-C), similar to the profile of Ndst1-induction. Furthermore, as with Ndst1 expression, no HS staining was detected within the lesion (Figure 2B-C). This staining is specific as it was absent after treatment with Heparinase, an enzyme that digests N-sulfated motifs on the HS chains [34] (Figure 2D). This correlation between *Ndst1* up-regulation and the presence of a highly N-sulfated microenvironment indicates the functional activity of Ndst1 after LPC-induced demyelination in the corpus callosum.

The phenotype of *Ndst1* expressing cells around the demyelinated lesion was examined at 5 dpi, using co-staining for several markers combined with *Ndst1* in situ hybridization. We found that *Ndst1* expressing cells are immunopositive for Olig2 (Figure 3A) and *Plp*+ using double in situ hybridization (Figure 3B). We quantified that 98.0±1.5% *Ndst1*+ cells express Olig2 indicating that virtually all *Nsdt1* cells belong to the oligodendroglia lineage. We found that Ndst1 expressing cells are immunopositive for Olig2, PDGFRα and CC1 (Figure 3A,C,D) and Plp+ using double in situ hybridization (Figure 3B*)* At 5 dpi, 97.5±1.7% of *Ndst1* expressing cells were co-labelled with CC1, a mature OLG marker (Figure 3D), while only 0.8±0.3% co-expressed the OPC marker PDGFRα (Figure 3C).

Of note, in the belt delimitated by *Ndst1* staining surrounding the lesion, only half of the Olig2+ cells expressed *Ndst1 (*45.8±3.4%). This may indicate that not all stages of oligodendroglial maturation or not all oligodendrocytes respond equally to the lesion. We

observed that, 8.5±3.2% of PDGFRα+ cells and 48.9±8.5% of CC1+ cells surrounding the lesion co-labelled with *Ndst1*. Our data indicate that the majority of Ndst1+ cells around the lesion are mature OLG which are more prone than OPC to activate Ndst1 expression in response to demyelination

Deletion of *Ndst1* in the Olig2+ population transiently worsens the extent of demyelination and modifies OPC reactivity after LPC injection.

To test if Ndst1 activity in oligodendroglia controls demyelination and/or remyelination, we generated transgenic mice with a conditional deletion of *Ndst1* in Olig2+ cells, by breeding *Olig2-Cre+/-* mice and *Ndst1* $^{Flox/Flox}$ mice [19, 35]. The efficiency of inactivation of *Ndst1* expression in Olig2 cells was monitored by in situ hybridization in the context of LPC-induced demyelinating lesion, revealing a drastic decrease in *Ndst1* expression in lesioned mutants compared to control (Figure 4-figure supplement 1A-D). As revealed by immunostaining using the anti-HS antibody, a strong reduction in N-sulfated HS positive puncta around the demyelination lesion was also observed in mutant compared to control (Figure 4-figure supplement 1G-H). In healthy mice, quantitative analysis of myelin content (Figure 4-figure supplement 2A-C; p=0.2), astrocyte density (Figure 4-figure supplement 2D-F; p=0.4) and oligodendroglial lineage cell density (Figure 4-figure supplement 2G-L; p=0.6, 0.2 and 0.2 for Olig2, CC1 and PDGFRα cell density respectively) revealed no difference between control (*Olig2-Cre+/-*) and mutant (*Olig2-Cre+/-; Ndst1* $^{Flox/Flox}$) adult mice, thus indicating that conditional deletion of *Ndst1* in the Olig2+ cell population does not interfere with brain development and with subsequent myelin maturation.

We first performed LPC-induced demyelination of the corpus callosum in control and mutant mice and measured the size of the lesion at 4, 8 and 14 dpi. As before, lesions were

identified based on the high density of nuclei at the injection point (Figure 1-figure supplement 2). While no difference was detected at 4 dpi (0.226±0.036 vs. 0.159±0.033 mm^3 in control and mutant mice, respectively; p=0.23), a significant two-fold increase in lesion size was observed in mutant compared to control mice at 8 dpi (0.199±0.032 vs. 0.097±0.022 mm^3, p=0.023) (Figure 4A-C). During the remyelination phase (between 8 and 14 dpi), the lesion area decreased in both groups reaching comparable sizes at 14 dpi (0.033±0.02 vs. 0.028±0.012 mm^3 in control and mutant mice, respectively; p=0.97) (Figure 4C).

We examined how these changes in the local environment in these mutant mice affect OPC mobilization during remyelination by analyzing Olig2+ cells density (Figure 4D-F), maturation status (Figure 4G-I) and proliferation (Figure 4J-O). In accordance with demyelination, there was a marked decrease in Olig2+ cell density within the demyelinated area compared to healthy corpus callosum in both groups at 4 dpi (55.5±3.3% and 57.3± 3.9% decrease in control and mutant mice respectively, p=0.03 and p=0.001) (Figure 4F), reflecting the loss of oligodendrocytes. We observe that in both conditions the density of Olig2+ cells returned to uninjected control values at 14 dpi. Quantification of mean cell densities of mature OLG (CC1+) (Figure 4G-I) within the lesion throughout the time course revealed no significant difference between the two groups indicating that cell differentiation is not affected by *Ndst1* inactivation.

We observed that the percentage of Ki67+ proliferating cells within the lesion area was two-fold increased in *Ndst1* mutant mice compared to control mice at 8 dpi (217.8±42.8% vs. 100±13.5% in mutant and control mice, respectively, p=0.037) (Figure 4J-K). Some of these proliferative cells are OPC since they co-express Olig2 and Ki67 (Figure 4M-O). At 4 dpi, the percentage of proliferating Olig2+ cells was lower (but not significantly different) in mutant mice compared to control (23±3.6% vs. 17±2.6% of Ki67+/Olig2+ cells in control and mutant mice, respectively, p=0.29) (Figure 4O). At 8 dpi, the percentage of proliferating

Olig2+ cells was significantly increased in mutant mice (7.6±0.8% vs 3.2±0.5% in mutant and control mice, respectively, p=0.0004) indicating a prolongation of OPC reactivity during the repair phase. These data show that OPC reactivity is altered in absence of Ndst1 at the onset of remyelination (8dpi). To note, no significant difference in cell death was detectable in the lesion between the two groups at 4 dpi (341.7±4.5 and 357±111.1 caspase3+ cells per mm² in control and mutant mice, respectively, p=0.28).

Together, these results suggest that *Ndst1* expression in the Olig2+ population has no effect on initial demyelination (equivalent lesion size at 4 dpi) but protects the lesion from enlarging and participates in the control of OPC mobilization.

Deletion of *Ndst1* in the Olig2+ population modulates microglia/macrophage activation.

While the total number of proliferating cells within the lesion area was strongly increased in *Ndst1* mutant mice compared to control mice at 8 dpi (Figure 4J-L), the percentage of OPC among these cells represent only 7.6% in the mutant. These data suggest that *Ndst1* loss in the Olig2 population indirectly modulates proliferation of surrounding cell types in the context of a demyelinating lesion. To address this, we evaluated the proliferation and activation states of the macrophage/microglia participating in demyelination-remyelination in this acute demyelination model. We found a robust increase in proliferation of CD68+ cells in mutant compared to control mice at 8 dpi (166.4±24.3 vs. 79.3±20.6 CD68+/Ki67+ cells per mm² in mutant and control mice, respectively, p=0.026) (Figure 5A-C). Upon CNS insult, microglia/macrophages are quickly activated, changing their shape from ramified to rhomboid. Rhomboid versus ramified polarization of total or activated microglia/macrophages was examined using respectively Iba1 (Figure 5D-E) and CD68 (Figure 5F-H) immunostaining. We observed a switch of the microglia/macrophage polarization among the whole Iba1 and CD68 population in favor of the rhomboid phenotype in mutant mice

compared to control at 8 dpi. This effect was quantified for activated microglia (ratio of rhomboid /ramified CD68+ cells of 0.28±0.05 in control vs. 0.66±0.1 in mutant mice, p=0.038) (Figure 5H). While the activation phenotype tended to decrease between 4 and 8 dpi in control mice, it tended to increase in mutant animals. We then evaluated the expression level of Cox2, a marker of pro-inflammatory (M1) microglia/macrophage [36] and observed a significant 77% increase in the number of Cox2+ microglial cells in mutant mice compared to control (p=0.01), indicating a delay in the pro-inflammatory (M1) to pro-regenerative (M2) switch in the absence of Ndst1 in oligodendroglia (Figure 5I-K). These results demonstrate that *Ndst1* deletion in the Olig2 population is sufficient to enhance microglia/macrophage proliferation and activation at the lesion site at the onset of remyelination.

Shh binds to HS around the focal LPC-induced demyelinated lesion in the corpus callosum

As previously mentioned, HSPGs form a scaffold that shapes the distribution and activity of numerous growth factors and morphogens during development and provide environmental support for regenerative responses following CNS injury. Among several known HSPG-binding morphogens, Shh was previously identified as a positive regulator for myelin repair [14, 29]. In order to determine whether lesion-induced HS enrichment around the lesion site could influence Shh distribution (hence signaling), we used an Alkaline Phosphatase (AP) tagged version of Shh (AP-SHH) to directly assay its binding capacity in demyelinating context. Knowing that the CW sequence serves as a major HS-binding site for Shh [37, 38], we also used AP-SHH recombinant proteins deleted for the CW sequence (AP-SHH-CWdeleted), as a control. Probes were incubated on fresh brain sections obtained 4 days after LPC injections. AP-Shh binding was observed in the cortex in healthy conditions (data not shown) and after lesion (Figure 6B,B'). While no AP-Shh binding was observed in healthy or

uninjured contralateral corpus callosum, AP-Shh binding delimited a clear belt surrounding the lesion site in the corpus callosum after LPC injection (Figure 6B-B'). In contrast, AP-Shh-CWdeleted did not bind around the same lesion on adjacent sections (Figure 6C-D). As AP-Shh binding depends on the integrity of its HS-binding motif, this indicates that endogenous Shh localization and concentration may be controlled by HS production by peri-lesional OLG. In order to assess whether SHH signaling was indeed reduced in *Ndst1* mutant mice compared to control mice, we quantified *Ptch1* (the main SHH receptor) expression around LPC-induced demyelination lesions at 8 dpi using RNAscope (Figure 6E-G). Ndst1 mutant mice exhibited 38% decrease in Ptch1 expression compared to control mice (8.6±0.7 vs 13.8±3.0 dots/cells in mutant and control mice respectively, n=5 mice/group) although it did not quite reach significance (p=0.07) (Figure 6E). Altogether these results suggest that lack of NDST1 in OLG lineage attenuates SHH signaling following demyelination insult.

NDST1 is expressed by oligodendroglia in multiple sclerosis lesions and correlates with lesion size and remyelination

To examine the relevance of our findings for multiple sclerosis (MS) physiopathology, we examined Ndst1 expression in MS tissue. We first probed the snRNAseq data provided by Jakel et al work [39], and observed that few cells express Ndst1 in both control and MS tissues but when the oligodendrocytes that express Ndst1 are compared, there is a trend to increased expression in MS tissue (Figure 7-figure supplement1). Because such approach identifies around 15% only of nuclear RNA, we then directly examined the expression pattern of NDST1 protein in MS patient brain sections. Normal appearing white matter (WM), remyelinating, active, chronic active or chronic inactive lesions were analyzed. While NDST1 staining was very weak in control WM (without MS), we observed a significant increase of NDST1 labeling in MS patients WM (Figure 7A-B). Comparison of healthy control, MS

normal appearing WM and MS lesions showed that there is a significant increase of NDST1 staining in multiple sclerosis lesions vs. control (p=0.0014) (Figure 7C). Comparison of each MS lesion with its surrounding normal appearing WM using a paired t test, revealed that there is significantly more NDST1 labeling in MS lesions compared to their surrounding normal appearing WM (paired two-tailed t test, t_9=3.39, p=0.0095). However, NDST1+ cells were distributed evenly throughout the lesion, rather than forming a delimiting band (Figure 7-figure supplement 2D).

We then performed double-labeling immunohistochemistry to characterize NDST1-positive cells in various types of lesions and normal appearing WM, using OLIG2 for oligodendroglia (Figure 7D), GFAP for astrocytes (Figure 7E), NEUN for neurons (Figure 7F) and IBA1 for microglia/macrophages (Figure 7G). Quantitative analysis showed that the majority of NDST1 cells were oligodendroglia in all types of lesions (remyelinated, active, chronic active, chronic inactive) and in normal appearing WM (Figure 7H).

The vast majority of OLIG2+ cells in the lesions expressed NDST1, with a gradual reduction in the proportion of OLIG2+NDST1+ cells as lesions become more chronic, and with significantly fewer in control tissue (Figure 7I; p=0.016). The number of NDST1+ oligodendroglia in each lesion was inversely correlated with the lesion's size (Figure 7J). As blocks of MS tissue contained multiple lesions and sometimes we had multiple blocks from the same patient (see Table1), we gave each patient an overall remyelination ability score corresponding to how many lesions in the blocks from that patient were remyelinated, or likely to remyelinate if the patient had survived. Here, we were aiming to see whether patients considered being "good remyelinators" using this score express more NDST1. A lesion was given a score of 3 points (complete remyelination), 2 points (active - likely to remyelinate), 1 point (chronic active less likely to remyelinate) and 0 points (chronic inactive -unlikely to remyelinate). The total score of all the lesions per patient was then divided by the number of

lesions per patient, to allow comparisons. We showed that NDST1+ cell density positively correlated with patient's score of remyelination ability (Figure 7K). These data reveal that MS tissues with a higher repair potential (containing most active and remyelinated lesions) display a high number of NDST1+ cells therefore suggesting that higher numbers of NDST1+ cells in a lesion may provide a positive environmental support for myelin repair.

DISCUSSION

In this study, we investigated the role of Ndst1 and HS after demyelination. Using LPC-induced demyelination of the corpus callosum in mouse, we showed for the first time that Ndst1-dependent N-sulfate sugar modifications occur at the onset of demyelination and during remyelination. These modifications limit the extension of demyelination and create a permissive substrate enhancing remyelination. First, we show that *Ndst1* is almost exclusively expressed by oligodendroglia present at the margin of the lesion delimiting the lesion from the intact corpus callosum. Second, we found that the conditional deletion of *Ndst1* in the Olig2 population concomitantly triggers an enlargement of the LPC-induced demyelinated area, alters OPC mobilization and favors the pro-inflammatory (M1) phenotype in microglia. We propose that these effects could be mediated through HS dependent binding of the morphogen Shh which has been shown to be a positive regulator of myelin repair through increased oligodendrogenesis and microglial regulation [14, 29]. Finally, using MS brain tissue samples, we show that NDST1 is up-regulated, especially within lesions and that the density of NDST1+ cells in these lesions is negatively correlated to lesion size, and positively correlated to the patient's potential remyelination ability. Our data suggest that Ndst1/HS expressed by oligodendrocytes around the lesion create a protective and permissive environment playing a positive role in myelin repair.

HS and chondroitin sulfates are the two main classes of sulfated proteoglycans constituting the extracellular space. Chondroitin sulfates are strongly expressed by astrocytes and microglia providing a hostile environment impeding regeneration and remyelination following brain injury [40-43]. Enzymatic degradation of chondroitin sulfate proteoglycans using chondroïtinase ABC treatment *in vivo* promotes OPC mobilization and remyelination [43]. In vitro, chondroitin sulfates reduce OPC maturation [44] and in vivo the use of a CSPG

synthesis inhibitor promotes OPC maturation and accelerates remyelination following focal demyelination in mice [45]. A recent study has shown that Surfen, a proteoglycan binding agent, reduces inflammation and delays remyelination. [46]. Our study provides evidence for a beneficial effect of HS proteoglycans (and upstream enzyme Ndst1) on limiting demyelinated lesion size and promoting remyelination. Here we propose that HS on mature OLG changes the amount/stability of soluble factors, and thus the recruitment and proliferation of surrounding cells (such as OPC or microglia). Thus, OLG modify their environment which in turn regulates the behavior of cells in the lesioned CC including microglia and OPC. Therefore, two classes of sulfated proteoglycans have opposite effects on myelin repair; one being detrimental (chondroitin sulfates), and the other (HS) having a beneficial effect. Interestingly, both are found at the margin of the lesion, but while the chondroitin sulfates are secreted by astrocytes and microglia, HS are expressed by oligodendroglia. Our data show that the majority of *Ndst1+* cells at the margin of the LPC-induced lesion are mature CC1+ OLG revealing that mature OLG around a demyelination lesion, respond to post lesional cues. Interesting, recent data have shown that pre-existing mature OLG can also participate to myelin regeneration in human and rodent by forming new myelin sheaths further indicating that mature OLG have an active role in myelin repair [47, 48].

This OLG response to nearby demyelination appears propitious to regeneration by restricting the lesion spread, favoring OPC mobilization and modulating microglia response.

Macrophages/microglia participate to myelin repair through myelin debris clearance and the secretion of regenerative factors that altogether promote the recruitment of OPC, their proliferation and differentiation into mature myelin-forming cells. Activated microglia also produces various pro-inflammatory mediators (cytokines, chemokines…) that may affect

OPC since they express a battery of receptors [49]. Recent studies have shown that efficient remyelination required the dynamic regulation of functional microglia phenotype [7, 50]. Microglia respond to demyelination with initial pro-inflammatory phenotype (M1) followed later by pro-regenerative phenotype (M2) which actively contributes to myelin repair [7, 51]. Interestingly, this transition from pro-inflammatory to pro-regenerative phenotype is a rate-limiting step in the repair process since intra-lesional depletion of pro-regenerative microglia blocks oligodendrocyte differentiation and delays the regenerative process [7]. In our study, lack of Ndst1/HS from Olig2+ cells in transgenic mice leads to increased microglial proliferation, a strongly activated rhomboid polarization of CD68-expressing cells and an increased density of pro-inflammatory (M1) microglia at an early stage of the remyelination phase (8 dpi). Altogether these effects may contribute to enlargement of the demyelinated lesion and delayed myelin repair. This non-cell autonomous effect observed on microglia activation could in turn disturb OPC mobilization and thus modify the repair process [7].

The beneficial action of HS may be related to their ability to bind numerous growth factors and morphogens, as observed during development [23]. HS can act as co-receptors for these ligands or are involved in the stabilization and/or local concentration of ligands in the extracellular space, which modulates cell signaling. Ndst1 global knock out mice display developmental defects that mainly resemble those found in embryos deficient for Shh or FGFs [52]. FGF and Shh implication in myelin regeneration and glial reactivation have been extensively examined in mouse models of demyelination (for review, see [8]). A role of both factors in remyelination was first inferred by correlating their spatial and temporal upregulation after demyelination particularly in LPC-induced demyelination [14, 53-55]
Concerning FGF, conflicting results have been published on its activity [56-61]. A recent report has addressed this issue using the simultaneous ablation of both FGFR1 and FGFR2

specifically in cells from the oligodendrocyte lineage [62]. This study revealed that FGF signaling is not required for myelin regeneration in acute models of demyelination including LPC-induced demyelination of the spinal cord and cuprizone intoxication [62]. Overall, in all these analyses the phenotypes observed after LPC-induced demyelination never recapitulate (even partially) the phenotype observed in the present report using *Olig2-Cre; Ndst1* $^{Flox/Flox}$ mice. This suggests that FGF is probably not the main ligand regulated by HS activity during myelin repair in this model.

By contrast, blocking Shh activity leads to an increase in demyelinated lesion size and an altered OPC mobilization after LPC-induced demyelination [14] similar to what we observe in *Olig2-Cre; Ndst1* $^{Flox/Flox}$ mice. However, these effects persist at later time points at the end of remyelination, and OPC maturation is also inhibited after Shh inactivation [14]. Of note, recent *in vitro* findings show that the proteolytic processing of Shh required for signaling pathway activation [63] is finely regulated by HS chains [64], perhaps influencing Shh concentration and/or spreading. Here we show that Shh binds to HS around demyelinated lesions in mouse. Thus, we propose that HS removal may delay the local accumulation around the demyelinated lesion of Shh produced by OLG [14] and/or delay Shh activation and spreading, leading to a reduction in signaling as suggested by reduced Ptch1 expression at early time-points. Later, the sustained production of Shh may overtake the absence of HS, leading to efficient recovery. Interestingly, Ferent et al. have shown that the main Shh responding cells (cells expressing Gli1 and/or Smo) after LPC-induced demyelination of the corpus callosum are OLG and microglia [14]. These observations further support the idea that sustained microglia and OPC activation in the absence of HS are at least in part due to altered Shh signaling.

Finally, we can confirm that NDST1 is also over-expressed in human MS brain samples, mostly in Olig2-positive oligodendroglia. High levels of HS proteoglycans and chondroitin

sulfate proteoglycans have been previously associated with inflammatory CNS diseases such as MS [65-68]. Here, we show that NDST1 is upregulated within and surrounding MS lesions in post mortem tissue compared to control. NDST1 expression is significantly higher in MS lesions compared to surrounding normal appearing white matter (NAWM), irrespective of lesion type (remyelinated, active, chronic active or chronic inactive). The distribution of the NDST+ cells was different from the mouse model, in that we saw no surrounding band of positive cells, but instead the entire lesions contained positive cells, though the majority of these cells were OLIG2+ oligodendroglia. This difference may be related to the timing of examination of the tissue after the lesion onset, which is later in the human tissue, and secondary to poorer repair in humans. In MS lesions, a large proportion of these OLIG2+ cells express NDST1, suggesting that at least some of these are mature, but we were unable to distinguish mature and immature oligodendroglia in this tissue (due to limitations in double-labelling using effective antibodies in human tissues). However, these observations still concur with our mouse data indicating that oligodendroglia respond to neighboring demyelination. Also consistent with our results showing increased lesion size in *Olig2-Cre+/- ; Ndst1* $^{Flox/Flox}$ mice, in human samples we observed an inverse correlation between lesion size and density of NDST1-expressing Olig2+ cells. NDST1 cell density also positively correlates with a pathological score of potential remyelination ability in patients.

Overall, our results in mouse and human tissues suggest that NDST1/HS levels are an indicator of oligodendroglial reactivity after demyelination, and are involved in both limiting the size of the lesion and creating a permissive environment for myelin regeneration. Furthermore, this study shows for the first time that mature oligodendrocytes around lesion are active players during demyelination/remyelination by producing HS and thus modifying the local environment. This study will help improve understanding the neuropathology of MS

in both limitation of damage and promotion of remyelination, which may in the future help target pharmacological approaches to potentiate myelin repair.

Acknowledgements

We are grateful to E. Traiffort, F Helmbacher and C. Bertet for critical reading of the manuscript.

MATERIALS AND METHODS

Key Resources Table				
Reagent type (species) or resource	**Designation**	**Source or reference**	**Identifiers**	**Additional information**
Genetic reagent (*M.musculus*)	*Olig2*^{Cre}	PMID:18046410		B6D2F1J/Rj genetic background
Genetic reagent (*M.musculus)*	*Ndst1*$^{flox/flox}$	PMID:16020517		Dr. Kay Grobe (University of Münster, Münster, Germany)
Genetic reagent (*M.musculus)*	*Plp*^{gfp}	PMID:15906234 PMID:11756747		Dr. Bernard Zalc (University of Sorbonne, Paris, France)
Biological sample (*H. Sapiens*)	Brain tissue from 9 MS patients	UK Multiple Sclerosis Tissue Bank (MREC/02/2/39)		Postmortem unfixed frozen
Biological sample (*H.*	Brain tissue from 4 Control	UK Multiple Sclerosis Tissue		Postmortem unfixed frozen

Sapiens)	patients	Bank (MREC/02/2/39)		
Cell line (*H. Sapiens*)	293T HEK	ATCC	CRL3216	
Transfected construct (*M.musculus*)	pWiz-AP-SHH	PMID: 16020517		Production of AP-tagged SHH recombinant protein
Transfected construct (*M.musculus*)	pWiz-AP-SHH-CWdeleted	PMID: 11959830		Production of AP-tagged deleted SHH recombinant protein
Antibody	Rabbit polyclonal anti-OLIG2	Millipore	AB9610	IF (1/1000)
Antibody	Rabbit polyclonal anti-OLIG2	Sigma-Aldrich	HPA003254	IF (1/100)
Antibody	Mouse monoclonal anti-APC (clone CC1)	Calbiochem	OP-80	IF (1/400)
Antibody	Rat monoclonal anti-PDGFRa (clone APA5)	Millipore	CBL1366	IF (1/250)
Antibody	Mouse monoclonal anti-MBP	Millipore	MAB384	IF (1/500)
Antibody	Mouse monoclonal anti-Ki67	BD Pharmingen	556003	IF (1/500)

Antibody	Rabbit polyclonal anti-Caspase 3	Cell Signalling	9661	IF (1/200)
Antibody	Rabbit polyclonal anti-GFAP	Dako	Z0334	IF (1/400)
Antibody	Goat polyclonal anti-IBA1	Abcam	Ab5076	IF (1/500)
Antibody	Rabbit polyclonal anti-IBA1	Wako Chemicals	019-19741	IF (1/500)
Antibody	Rat monoclonal Anti-CD68	Abcam	Ab53444	IF (1/400)
Antibody	Rabbit polyclonal anti-COX2	Abcam	Ab15191	IF (1/400)
Antibody	Mouse monoclonal IgM anti-N-sulfated motifs on HS chains (clone10E4)	Amsbio	370255-1	IF (1/500)
Antibody	Mouse monoclonal anti-NDST1	Abcam	ab55296	IF (1/50)
Antibody	Rabbit polyclonal anti-NeuN	Abcam	Ab104225	IF (1/500)
Sequence-based reagent	*Ndst1_F*	Eurofins Genomics	RT-qPCR primers	gctggacaagatcatcaatgg

Sequence-based reagent	*Ndst1_R*	Eurofins Genomics	RT-qPCR primers	acacagtacttctacgactatcc
Sequence-based reagent	*Gapdh_F*	Eurofins Genomics	RT-qPCR primers	gggttcctataaatacggactgc
Sequence-based reagent	*Gapdh_R*	Eurofins Genomics	RT-qPCR primers	ctggcactgcacaagaagat
Sequence-based reagent	*plp/dm20*	PMID:9373029		Probe for ISH
Sequence-based reagent	*Ndst1*	PMID:16020517		Probe for ISH
Sequence-based reagent	*Ptch1*	Advanced Cell Diagnostics	402811-C2	Probe for RNAScope
Peptide, Recombinant Protein	Human NDST1	Abcam	ab116875	
Commercial assay or kit	RNAscope Multiplex Fluorescent kit	Advanced Cell Diagnostics	323133	
Commercial assay or kit	DAB Peroxidase (HRP) Substrate Kit (with Nickel)	Vector Laboratories	SK-4100	
Commercial assay or kit	VECTOR Blue AP Substrate Kit	Vector Laboratories	SK-5300	
Commercial assay or kit	ImmPRESS™-AP Anti-Rabbit IgG Polymer Detection Kit	Vector Laboratories	MP-5401	

Commercial assay or kit	ImmPRESS™ HRP Anti-Mouse IgG Polymer Detection Kit	Vector Laboratories	MP-7402	
Chemical compound, drug	Lysolecithin	Sigma-Aldrich-Merck	L1381	
Chemical compound, drug	Heparinase	Amsbio	100700	
Chemical compound, drug	Lipofectamine 2000	Invitrogen	11668-030	
Chemical compound, drug	Vector Bloxall	Vector Laboratories	SP-6000	
Software, algorithm	ImageJ	https://imagej.nih.gov/ij/		
Software, algorithm	Zen 2 lite	Zeiss		
Software, algorithm	GraphPad Prism	https://graphpad.com		

Animals and treatments

All experimental and surgical protocols were performed following the guidelines established by the French Ministry of Agriculture (Animal Rights Division). The architecture and functioning rules of our animal house, as well as our experimental procedures have been approved by the ‘‘Direction Départementale des Services Vétérinaires’’ and the ethic

committee (ID numbers F1305521 and 2016071112151400 for animal house and research project,

respectively).. Surgery and perfusions were performed under ketamine (100 mg/kg, MERIAL, Lyon, France))/xylazine (10 mg/kg, BAYER, Puteaux, France) anesthesia. C57BL/6 wild-type and transgenic mice were successively used to characterize post-lesional expression of *Ndst1* and HS after demyelination and to investigate the impact of conditional deletion of *Ndst1* in the Olig2-positive cell population. Heterozygous *Olig2-Cre+/-* (from B6D2F1J/Rj genetic background) [35] and double transgenic *Olig2-Cre+/-; Ndst1* $^{Flox/Flox}$ mice [19, 35] will be referred below as control and mutant mice, respectively. Mice expressing GFP under the control of the proteolipid protein (plp, a protein largely present in myelin) promoter were used in some experiments to better observe demyelination lesions (called thereafter *plpGFP* mice). Animals were housed under standard conditions with enrichment and access to water and food *ad libitum* on a normal 12 h light/dark cycle.

Human postmortem samples

Postmortem unfixed frozen tissues were obtained from the UK Multiple Sclerosis Tissue Bank via a UK prospective donor scheme with full ethical approval (MREC/02/2/39). Luxol fast blue (LFB) (staining myelin; Figure7 -figure supplement 2C) and Oil Red O (staining lipids phagocytosed by macrophages) were performed to characterize and classify the lesion types [3]. Active lesions have indistinct borders on LFB and lipid-laden macrophages/microglia. Chronic active lesions have a ring of lipid-laden macrophages/microglia and a core with few immune cells. Chronic inactive lesions have a distinct border on LFB and few immune cells. Finally, shadow plaques, thought to represent remyelination, have less intense staining on LFB. This classification was done by two independent researchers for a previous publication [3]. In this study, we used active (n=7),

chronic active (n=4), chronic inactive (n=14) and remyelinated (shadow) MS plaques (n=21) from 14 blocks of brain tissue from 9 MS patients and 4 blocks of brain tissue from 4 controls with no neurological disease (Table 1)

Focal demyelination in the corpus callosum and tissue processing

Focal demyelination was performed by stereotactic injection of Lysolecithin (LPC) (SIGMA-ALDRICH, St Louis, USA) as described previously [30, 69]. The corpus callosum from healthy or demyelinated mice, from the ipsilateral and contralateral side to the LPC-induced lesion, were dissected 7 days post injection (dpi) from 1 mm thick coronal slices in cold Hank's Balanced Salt Solution (GIBCO by life technologie, Paisley, UK) and processed for RT-qPCR analysis (*Ndst1 primers : exon 6* (forward, 5′-gctggacaagatcatcaatgg-3′) and exon 7 (reverse, 5′-acacagtacttctacgactatcc-3′); for *Gapdh* : exon1 (forward, 5'-gggttcctataaatacggactgc-3') and exon2 (reverse 5'-ctggcactgcacaagaagat-3'). Primers from EUROFINS GENOMICS, Ebersberg, GERMANY). For histological analysis, mice were anesthetized and perfused with ice-cold 4% paraformaldehyde (FISHER SCIENTIFIC, Loughborough Leics, UK) in PBS (GIBCO by life technologie, Paisley, UK). Brains were post-fixed overnight in 4% paraformaldehyde in PBS and cut on a vibratome (Leica) in 4 series of coronal sections (50 µm thick) for immunofluorescence, or cryopreserved and cut with cryostat (20 µm thick) for in situ hybridization.

In situ hybridization and immunohistochemistry.

In situ hybridization was performed using *plp/dm20* [70] and *Ndst1* probes [19] as described in [71]. RNAscope Multiplex Fluorescent kit (323133; Advanced Cell Diagnostics) was used to detect Ptch1 mouse mRNA. Briefly cryosections were baked for 30 min at 60°C and dehydrated, incubated for 30min at 40°C with protease III before incubation with RNAScope

probe Ptch1 (402811-C2) for 2 hrs at 40°C. Immunohistochemistry was performed as described in [30]. The following primary antibodies were used: rabbit anti-Olig2 (AB9610; 1/1000, Millipore, USA), mouse anti-APC (CC1) (1/400; Calbiochem, USA), and rat anti-PDGFRα (CBL1366; 1/250; Millipore, USA) for oligodendroglial lineage cells; anti-MBP (mouse, 1/500, Chemicon, Millipore S.A.) for myelin sheaths; mouse anti-Ki67 (556003; 1/500; BD Pharmingen) for proliferating cells; rabbit anti-caspase 3 (9661; 1/200; Cell Signaling) for apoptotic cells, rabbit anti-GFAP (1/400) for astrocytes; goat anti-Iba1 (1/500, Abcam) for microglia and macrophages; rat anti-CD68 (1/400, Abcam) for activated microglia and macrophages; rabbit anti-Cox2 (1/400, Abcam) for proinflammatory M1 microglia/macrophage; mouse IgM anti-N-sulfated motifs on HS chains (10E4 antibody, 1/500; Seikagaku, Japan). For Olig2 and Ki67 immunofluorescence, antigen unmasking was performed by 20 min incubation in boiling citrate buffer (10mM pH6). For N-sulfated motifs labeling, floating sections from PFA perfused-brain were incubated for 2 h 30 at 37°C in buffer (100 mM Sodium Chloride, 1 mM Calcium Chloride, 50 mM Hepes 5µg, BSA pH 7) with or without Heparinase (3.3 mU from Flavobacterium heparinum, Seikagaku Kogyo Co. # 100700, Japan) [34] before permeabilization. Secondary antibodies coupled to alexa 488, 555 and 647 (1/500, Invitrogen Molecular Probes) were applied for 2 h 30 at RT in a humid chamber. Sections were counterstained with Hoechst 33342 (1/500, Sigma).

AP-Shh recombinant protein binding test in mice

Plasmids containing sequences for AP-tagged N-terminal WT or deleted Shh were produced by PCR and ligated into pWIZ vector as described in [19, 38]. Briefly, plasmids were transiently transfected into HEK cells using lipofectamine 2000 (Invitrogen). Transfection proceeded for 3 h. Culture supernatants were collected after 60 h and filtered through 0.45µm filters (Corning Incorporated, Durham, USA). Hepes 10mM pH7 was added to increase

stability. Shh concentration was then evaluated measuring AP activity in culture supernatants. Preparations from mock-transfected HEK cells were generated and used as vehicle controls. The AP-Shh binding test was performed as described in [38].

Fresh frozen brain sections were post-fixed with ice-cooled methanol for 8 min. After rinsing with phosphate-buffered saline containing 4mM MgCl2 and blocking with 1% Bovine Serum Albumin (SIGMA-ALDRICH, St Louis, MO, USA) 1 h at RT, frozen adjacent sections from healthy or demyelinated C57BL/6 mice were incubated with 5nM of two AP tagged versions of Shh: AP-Shh recombinant proteins carrying the N-terminal CW sequence (AP-SHH), the main HS-binding site for Shh [38] [37], or lacking this motif (AP-SHH-CWdeleted). Sections were then washed with PBS to dissociate any low affinity interaction and endogenous phosphatases were inactivated by heating at 65°C for 2 h. AP was revealed by incubating overnight in NBT (100mg/ml) /BCIP (50mg/ml) in 100mM Tris pH 9,5 with 100mM NaCl and 50mM MgCl2.

Immunohistochemistry on human post-mortem tissue

Tissue was fixed in 4% paraformaldehyde in PBS for 30 min. Endogenous peroxidase and AP activity was blocked by 10 min incubation with Vector Bloxall (Vector, SP-6000 VECTOR LABORATORIES, Burlingame, USA). Slides were blocked with ready-to-use 2.5% normal horse serum from Vector secondary antibody kits for at least 20 min. Primary antibodies were incubated overnight in antibody diluent (Spring Bioscience, ADS-125) at 4°C. Primary antibodies used: mouse anti-NDST1 (1/50; Abcam, ab55296), rabbit anti-NeuN (1/500; Abcam, ab104225), rabbit anti-IBA1 (1/500; Wako chemicals, 019-19741), rabbit anti-Olig2 (1/100; Sigma, HPA003254). HS staining with the mouse IgM anti-N-sulfated motifs on HS chains (10E4 antibody, Seikagaku, Japan) did not give any signal on human tissue. NDST1 intensity was evaluated after a short exposition (exactly 2 min). All other stainings were fully

developed. To ensure antibody specificity, the NDST1 antibody was pre-absorbed with human NDST1 recombinant protein (Abcam, ab116875), and added to tissue sections, with no staining seen (Figure7 -figure supplement 2A-B).

Secondary antibodies were incubated at RT for 1h. Staining was developed with a DAB Peroxidase (HRP) Substrate Kit (with Nickel), 3,3'-diaminobenzidine (Vector, SK-4100) and a VECTOR Blue AP Substrate Kit (Vector, SK-5300) as per manufacturer's guidelines. Secondary antibodies used: ImmPRESS™-AP Anti-Rabbit IgG Polymer Detection Kit (Vector, MP-5401) and ImmPRESS™ HRP Anti-Mouse IgG Polymer Detection Kit, made in Horse (Vector, MP-7402). PBS washes were performed between each treatment.

Microscopy and quantification

For mouse tissue analysis, imaging was performed with the Apotome system (Zeiss). The demyelinated area and cell counts were evaluated using Zen software (Zeiss). Immunofluorescent or in situ hybridization positive cells were counted in every fourth section through the whole demyelinated lesion per mouse and averaged for each mouse. Cell counts are presented as the mean of at least 3 mice. For RNAscope ISH, each punctate dot signal was counted around lesion (by using ROI and analyze particule Fiji Plugins) and reported to total nuclei number. Lesion size was quantified by measuring the area of high density of nuclei in every fourth section through the whole demyelinated lesion per mouse. In this analysis, high density of nuclei was correlated with myelin loss visualized by MBP staining or by loss of fluorescence in *plpGFP* mice (Figure1 -figure supplement 2).

For the human post-mortem tissue analysis, slides were imaged using a ZEISS Axio Scan.Z1 slide scanner. One researcher marked out the lesion sites and normal appearing white matter (WM) as areas of interest, while another counted single positive (NDST1+ cells) and double

positive cells (NDST+ cells and other brain cell markers combined as above) in these areas of interest (ensuring blinding of counting).

Myelin content was evaluated by double blind scoring of images taken from Plp immunostaining on brain sections (3 photos per section and 3 sections per brain). Score of 4 was attributed to maximum myelination down to 0 for absence of myelin. The mean score for the control group was considered as 100%.

Gene expression profile of demyelinated versus healthy mouse progenitors

This protocol is fully described in Cayre et al. [30]. Briefly, OPC from eight mice induced for experimental autoimmune encephalomyelitis (EAE mice) at the peak of paralytic symptoms and from eight adult healthy mice as controls were purified using magnetic cell sorting (Miltenyi Biotec). This experiment was replicated in an independent similar experiment. cDNAs were prepared and used (250 ng) as template for Cy3 and Cy5, combined and hybridized to Agilent Whole Mouse Genome Oligo Microarrays 4Å~44K. Agilent Feature Extraction Software (FES) determines feature intensities and ratios (including background subtraction and normalization), rejects outliers and calculates statistical confidences (P-values). We obtained a gene list with all normalized Cy5/Cy3 log10 ratios, Cy5/Cy3 fold changes, sequence description and P-values. Microarray data are available at GEO with accession number GSE47486.

Statistical analysis

All the presented values in mice are means ± S.E.M unless otherwise stated. Data were statistically processed with the non-parametric Mann-Whitney test (independent two group comparisons). $P<0.05$ was considered significant and $p<0.01$ highly significant. All measurements and subsequent evaluations were performed blind to the experimental group to

612 which the animals belonged. For the human post-mortem tissue analysis, a d'Agostino and
613 Pearson omnibus normality test was used to test whether the data fits a normal distribution
614 and a parametric test were done only if all compared data sets passed the normality test. The
615 NDST1+ cells in control versus multiple sclerosis WM was compared using a two-tailed
616 Mann Whitney U test. Multiple sclerosis lesions and their surrounding WM were compared
617 using a paired two-tailed t test. The absolute numbers of NDST1+ cells and double positive
618 NDST1+ OLIG2+ cells in individual lesions/normal appearing WM were compared by
619 Kruskal-Wallis test. As MS tissue blocks contained more than one lesion, and we had several
620 blocks from the same patients, we gave each patient an overall remyelination ability score
621 corresponding to how many lesions in the blocks from that patient were remyelinated, or
622 likely to remyelinate if the patient had survived. Remyelinated lesions received an arbitrary 3
623 points, active lesions 2 points, chronic active lesions 1 point and chronic inactive lesions 0
624 points. This was divided by the number of lesions counted for each patient, to allow
625 comparisons.

REFERENCES

1. Franklin, R.J. and C. Ffrench-Constant, *Remyelination in the CNS: from biology to therapy.* Nat Rev Neurosci, 2008. **9**(11): p. 839-55.
2. Patrikios, P., et al., *Remyelination is extensive in a subset of multiple sclerosis patients.* Brain, 2006. **129**(Pt 12): p. 3165-72.
3. Boyd, A., H. Zhang, and A. Williams, *Insufficient OPC migration into demyelinated lesions is a cause of poor remyelination in MS and mouse models.* Acta Neuropathol, 2013. **125**(6): p. 841-59.
4. Wolswijk, G., *Oligodendrocyte regeneration in the adult rodent CNS and the failure of this process in multiple sclerosis.* Prog Brain Res, 1998. **117**: p. 233-47.
5. Chang, A., et al., *Premyelinating oligodendrocytes in chronic lesions of multiple sclerosis.* N Engl J Med, 2002. **346**(3): p. 165-73.
6. Franklin, R.J., *Remyelination of the demyelinated CNS: the case for and against transplantation of central, peripheral and olfactory glia.* Brain Res Bull, 2002. **57**(6): p. 827-32.
7. Miron, V.E., et al., *M2 microglia and macrophages drive oligodendrocyte differentiation during CNS remyelination.* Nat Neurosci, 2013. **16**(9): p. 1211-8.
8. El Waly, B., et al., *Oligodendrogenesis in the normal and pathological central nervous system.* Front Neurosci, 2014. **8**: p. 145.
9. Emery, B., *Regulation of oligodendrocyte differentiation and myelination.* Science, 2006. **330**(6005): p. 779-82.
10. Aguirre, A., et al., *A functional role for EGFR signaling in myelination and remyelination.* Nat Neurosci, 2007. **10**(8): p. 990-1002.
11. Williams, A., et al., *Semaphorin 3A and 3F: key players in myelin repair in multiple sclerosis?* Brain, 2007. **130**(Pt 10): p. 2554-65.
12. Courtes, S., et al., *Reelin controls progenitor cell migration in the healthy and pathological adult mouse brain.* PLoS One, 2011. **6**(5): p. e20430.
13. Vernerey, J., et al., *Ciliary neurotrophic factor controls progenitor migration during remyelination in the adult rodent brain.* J Neurosci, 2013. **33**(7): p. 3240-50.
14. Ferent, J., et al., *Sonic Hedgehog signaling is a positive oligodendrocyte regulator during demyelination.* J Neurosci, 2013. **33**(5): p. 1759-72.
15. Sarrazin, S., W.C. Lamanna, and J.D. Esko, *Heparan sulfate proteoglycans.* Cold Spring Harb Perspect Biol, 2011. **3**(7).
16. Lindahl, U., M. Kusche-Gullberg, and L. Kjellen, *Regulated diversity of heparan sulfate.* J Biol Chem, 1998. **273**(39): p. 24979-82.
17. Perrimon, N. and M. Bernfield, *Specificities of heparan sulphate proteoglycans in developmental processes.* Nature, 2000. **404**(6779): p. 725-8.
18. Carlsson, P., et al., *Heparin/heparan sulfate biosynthesis: processive formation of N-sulfated domains.* J Biol Chem, 2008. **283**(29): p. 20008-14.
19. Grobe, K., et al., *Cerebral hypoplasia and craniofacial defects in mice lacking heparan sulfate Ndst1 gene function.* Development, 2005. **132**(16): p. 3777-86.
20. Pallerla, S.R., et al., *Heparan sulfate Ndst1 gene function variably regulates multiple signaling pathways during mouse development.* Dev Dyn, 2007. **236**(2): p. 556-63.
21. Matsuo, I. and C. Kimura-Yoshida, *Extracellular distribution of diffusible growth factors controlled by heparan sulfate proteoglycans during mammalian embryogenesis.* Philos Trans R Soc Lond B Biol Sci, 2014. **369**(1657).
22. Gallagher, J.T., *Heparan sulfate: growth control with a restricted sequence menu.* J Clin Invest, 2001. **108**(3): p. 357-61.

23. Hacker, U., K. Nybakken, and N. Perrimon, *Heparan sulphate proteoglycans: the sweet side of development.* Nat Rev Mol Cell Biol, 2005. **6**(7): p. 530-41.
24. Parker, R.B. and J.J. Kohler, *Regulation of intracellular signaling by extracellular glycan remodeling.* ACS Chem Biol, 2010. **5**(1): p. 35-46.
25. Iseki, K., et al., *Increased syndecan expression by pleiotrophin and FGF receptor-expressing astrocytes in injured brain tissue.* Glia, 2002. **39**(1): p. 1-9.
26. Hagino, S., et al., *Slit and glypican-1 mRNAs are coexpressed in the reactive astrocytes of the injured adult brain.* Glia, 2003. **42**(2): p. 130-8.
27. McKinnon, R.D., et al., *FGF modulates the PDGF-driven pathway of oligodendrocyte development.* Neuron, 1990. **5**(5): p. 603-14.
28. Bansal, R. and S.E. Pfeiffer, *Regulation of oligodendrocyte differentiation by fibroblast growth factors.* Adv Exp Med Biol, 1997. **429**: p. 69-77.
29. Zakaria, M., et al., *The Shh receptor Boc is important for myelin formation and repair.* Development, 2019. **146**(9).
30. Cayre, M., et al., *Netrin 1 contributes to vascular remodeling in the subventricular zone and promotes progenitor emigration after demyelination.* Development, 2013. **140**(15): p. 3107-17.
31. Spassky, N., et al., *The early steps of oligodendrogenesis: insights from the study of the plp lineage in the brain of chicks and rodents.* Dev Neurosci, 2001. **23**(4-5): p. 318-26.
32. Le Bras, B., et al., *Oligodendrocyte development in the embryonic brain: the contribution of the plp lineage.* Int J Dev Biol, 2005. **49**(2-3): p. 209-20.
33. Pan, Y., et al., *Heparan sulfate expression in the neural crest is essential for mouse cardiogenesis.* Matrix Biol, 2014. **35**: p. 253-65.
34. David, G., et al., *Developmental changes in heparan sulfate expression: in situ detection with mAbs.* J Cell Biol, 1992. **119**(4): p. 961-75.
35. Dessaud, E., et al., *Interpretation of the sonic hedgehog morphogen gradient by a temporal adaptation mechanism.* Nature, 2007. **450**(7170): p. 717-20.
36. Chhor, V., et al., *Role of microglia in a mouse model of paediatric traumatic brain injury.* Brain Behav Immun, 2017. **63**: p. 197-209.
37. Carrasco, H., et al., *Heparan sulfate proteoglycans exert positive and negative effects in Shh activity.* J Cell Biochem, 2005. **96**(4): p. 831-8.
38. Rubin, J.B., Y. Choi, and R.A. Segal, *Cerebellar proteoglycans regulate sonic hedgehog responses during development.* Development, 2002. **129**(9): p. 2223-32.
39. Jakel, S., et al., *Altered human oligodendrocyte heterogeneity in multiple sclerosis.* Nature, 2019. **566**(7745): p. 543-547.
40. Siebert, J.R. and D.J. Osterhout, *The inhibitory effects of chondroitin sulfate proteoglycans on oligodendrocytes.* J Neurochem, 2011. **119**(1): p. 176-88.
41. Pendleton, J.C., et al., *Chondroitin sulfate proteoglycans inhibit oligodendrocyte myelination through PTPsigma.* Exp Neurol, 2013. **247**: p. 113-21.
42. Deng, Y.P., et al., *Chondroitin sulfate proteoglycans impede myelination by oligodendrocytes after perinatal white matter injury.* Exp Neurol, 2015. **269**: p. 213-23.
43. Lau, L.W., et al., *Chondroitin sulfate proteoglycans in demyelinated lesions impair remyelination.* Ann Neurol, 2012. **72**(3): p. 419-32.
44. Karus, M., et al., *Regulation of oligodendrocyte precursor maintenance by chondroitin sulphate glycosaminoglycans.* Glia, 2016. **64**(2): p. 270-86.
45. Keough, M.B., et al., *An inhibitor of chondroitin sulfate proteoglycan synthesis promotes central nervous system remyelination.* Nat Commun, 2016. **7**: p. 11312.

46. Warford, J.R., et al., *Surfen, a proteoglycan binding agent, reduces inflammation but inhibits remyelination in murine models of Multiple Sclerosis.* Acta Neuropathol Commun, 2018. **6**(1): p. 4.
47. Yeung, M.S.Y., et al., *Dynamics of oligodendrocyte generation in multiple sclerosis.* Nature, 2019. **566**(7745): p. 538-542.
48. Duncan, I.D., et al., *The adult oligodendrocyte can participate in remyelination.* Proc Natl Acad Sci U S A, 2018. **115**(50): p. E11807-E11816.
49. Peferoen, L., et al., *Oligodendrocyte-microglia cross-talk in the central nervous system.* Immunology, 2014. **141**(3): p. 302-13.
50. Lloyd, A.F., et al., *Central nervous system regeneration is driven by microglia necroptosis and repopulation.* Nat Neurosci, 2019. **22**(7): p. 1046-1052.
51. Olah, M., et al., *Identification of a microglia phenotype supportive of remyelination.* Glia, 2012. **60**(2): p. 306-21.
52. Pallerla, S.R., et al., *Altered heparan sulfate structure in mice with deleted NDST3 gene function.* J Biol Chem, 2008. **283**(24): p. 16885-94.
53. Gudi, V., et al., *Spatial and temporal profiles of growth factor expression during CNS demyelination reveal the dynamics of repair priming.* PLoS One, 2011. **6**(7): p. e22623.
54. Hinks, G.L. and R.J. Franklin, *Distinctive patterns of PDGF-A, FGF-2, IGF-I, and TGF-beta1 gene expression during remyelination of experimentally-induced spinal cord demyelination.* Mol Cell Neurosci, 1999. **14**(2): p. 153-68.
55. Tourbah, A., et al., *Endogenous aFGF expression and cellular changes after a demyelinating lesion in the spinal cord of adult normal mice: immunohistochemical study.* J Neurosci Res, 1992. **33**(1): p. 47-59.
56. Ruffini, F., et al., *Fibroblast growth factor-II gene therapy reverts the clinical course and the pathological signs of chronic experimental autoimmune encephalomyelitis in C57BL/6 mice.* Gene Ther, 2001. **8**(16): p. 1207-13.
57. Dehghan, S., et al., *Basic fibroblast growth factor potentiates myelin repair following induction of experimental demyelination in adult mouse optic chiasm and nerves.* J Mol Neurosci, 2012. **48**(1): p. 77-85.
58. Kumar, S., et al., *Combination of growth factors enhances remyelination in a cuprizone-induced demyelination mouse model.* Neurochem Res, 2007. **32**(4-5): p. 783-97.
59. Armstrong, R.C., et al., *Absence of fibroblast growth factor 2 promotes oligodendroglial repopulation of demyelinated white matter.* J Neurosci, 2002. **22**(19): p. 8574-85.
60. Zhou, Y.X., et al., *Fibroblast growth factor 1 (FGFR1) modulation regulates repair capacity of oligodendrocyte progenitor cells following chronic demyelination.* Neurobiol Dis, 2012. **45**(1): p. 196-205.
61. Kang, W., K.C.Q. Nguyen, and J.M. Hebert, *Transient Redirection of SVZ Stem Cells to Oligodendrogenesis by FGFR3 Activation Promotes Remyelination.* Stem Cell Reports, 2019. **12**(6): p. 1223-1231.
62. Furusho, M., et al., *Fibroblast growth factor signaling in oligodendrocyte-lineage cells facilitates recovery of chronically demyelinated lesions but is redundant in acute lesions.* Glia, 2015. **63**(10): p. 1714-28.
63. Ohlig, S., et al., *An emerging role of Sonic hedgehog shedding as a modulator of heparan sulfate interactions.* J Biol Chem, 2012. **287**(52): p. 43708-19.
64. Ortmann, C., et al., *Sonic hedgehog processing and release are regulated by glypican heparan sulfate proteoglycans.* J Cell Sci, 2015. **128**(12): p. 2374-85.

65. Briani, C., et al., *Anti-heparan sulfate antibodies in neurological disease.* Muscle Nerve, 2002. **26**(5): p. 713-5.
66. Berezin, V., et al., *Targeting of ECM molecules and their metabolizing enzymes and receptors for the treatment of CNS diseases.* Prog Brain Res, 2014. **214**: p. 353-88.
67. van Horssen, J., et al., *Extensive extracellular matrix depositions in active multiple sclerosis lesions.* Neurobiol Dis, 2006. **24**(3): p. 484-91.
68. Satoh, J.I., H. Tabunoki, and T. Yamamura, *Molecular network of the comprehensive multiple sclerosis brain-lesion proteome.* Mult Scler, 2009. **15**(5): p. 531-41.
69. Magalon, K., et al., *Enriched environment promotes adult neural progenitor cell mobilization in mouse demyelination models.* Eur J Neurosci, 2007. **25**(3): p. 761-71.
70. Peyron, F., et al., *In situ expression of PLP/DM-20, MBP, and CNP during embryonic and postnatal development of the jimpy mutant and of transgenic mice overexpressing PLP.* J Neurosci Res, 1997. **50**(2): p. 190-201.
71. Virard, I., et al., *Oligodendrocyte precursor cells generate pituicytes in vivo during neurohypophysis development.* Glia, 2006. **53**(3): p. 294-303.

Figure 1. *Ndst1* up-regulation upon LPC-induced demyelination of the corpus callosum. **(A)** Scheme showing the site of LPC injection (red point) in the adult corpus callosum and the location of picture shown in C (red rectangle). **(B)** *Ndst1* expression levels (RT-qPCR) in the corpus callosum of healthy or demyelinated mice, contralateral (contra) and ipsilateral (ipsi) to the lesion site showing the *Ndst1* up-regulation in the ipsilateral side. Tissues from 5 mice were pooled in each condition. Error bars represent S.E.M. *p<0.05, non-parametric ANOVA followed by Kruskal-Wallis test (independent two group comparisons). **(C-H)** *Ndst1* in situ hybridization performed at 5 **(C-F**, n=4**)**, 8 **(G**, n=4**)** and 14 **(H**, n=4**)** dpi illustrating the *Ndst1* expression pattern at different time points of demyelination **(C-F)** and remyelination **(G-H)**. **(D-E)** Enlarged views of the CC in **C** corresponding to contralateral side **(D)** and positive cells at the margin of the demyelinated area at the site of LPC injection **(E)**. CC, corpus callosum; Cx, cortex; SVZ, sub-ventricular zone; V, ventricle (structures are delineated by brown dotted lines, lesion with white dotted lines). Scale bars: 50 µm in F, G and H; 20 µm in D, F, H; 10 µm in D and E Asterisk in G indicates the site of injection since the demyelinated lesion is no longer visible at 14 dpi.

Figure 1-figure supplement 1. *Ndst1* is up-regulated by the Olig2+ cell population in close proximity to inflammation sites in corpus callosum, in the experimental autoimmune encephalomyelitis mouse model of demyelination. *Ndst1* is not expressed in control brain **(A)** (n=2) while it is up-regulated by Olig2+ cells after experimental autoimmune encephalomyelitis induction **(B)**(n=3) in close proximity to lesions in the corpus callosum **(C).** Enlarged views correspond to boxed region. CC, corpus callosum. Scale bars: 50 µm in A-B; 20 µm in C.

Figure 1 Supplement 2. *PlpGFP* mice (n=3) were used to detect demyelinated lesions (A, B, D, E). Demyelination was clearly visible in the corpus callosum around the injection site by the lack of GFP fluorescence (B, E). Hoechst staining shows a high cell density (C, F) correlating with the loss of myelin (A, D). CC, corpus callosum, Cx, cortex, V, ventricle, St, Striatum. Scale bars: 100 µm.

Figure 2. N-sulfate-enriched microenvironment forms a belt around the demyelinated lesion. HS (10E4) labeling on the contra- **(A)** and ipsi- **(B-C)** lateral side to the lesion illustrates the generation of a N-sulfated microenvironment surrounding the lesion (delimited by white dashed lines) at 5 dpi (n=3). No immunoreactivity was found after Heparinase I treatment **(D)** thus validating the 10E4 antibody specificity. Scale bars: 20 µm in A, B, D; 10 µm in C. CC, corpus callosum; V, ventricle.

Figure 3. Ndst1 expressing cells around the lesion belong to the oligodendroglial lineage. **(A-B)** *Ndst1* in situ hybridization successively combined with Olig2 immunostaining **(A)** or *Plp* in situ hybridization **(B)** labeling, two OLG markers, illustrating *Ndst1* up-regulation in

oligodendroglia lineage cells surrounding the lesion site at 5 dpi (n=3). **(C-D)** Representative images of *Ndst1*/PDGFRα **(C)** and *Ndst1*/CC1 **(D)** co-labeling illustrating that both OPC **(C)** and mature OLG **(D)** up-regulate *Ndst1* after demyelination at 5 dpi (n=4). Inserts in **(A-D)** illustrate boxed regions at high magnification. Scale bars: 20 µm**.**

Figure 4. Deletion of *Ndst1* in Olig2+ cells affects lesion size and OPC mobilization after LPC-induced demyelination of the corpus callosum.

(A-B) Representative images of the lesion site (delineated by white dashed lines) in the corpus callosum of control **(A)** and mutant **(B)** mice at 8 dpi illustrating the enlargement of the lesion size in mutant mice compared to control mice. **(C)** Quantitative analysis of the lesion size at 4, 8 and 14 dpi (n=8,9,4 control and n=9,12,6 mutant mice respectively). **(D-E)** Oligodendroglia labeled by Olig2 staining within the demyelinated area at 8 dpi **(E)** compared to control mice **(D)**. **(F)** Olig2 mean cell density in healthy (CTL) or demyelinated control and mutant mice at 4, 8, 14 dpi. **(G-H)** Mature OLG co-labeled by Olig2/CC1 within the demyelinated lesion at 8 dpi in control **(G)** and mutant **(H)** mice. **(I)** Quantification of mean cell density of Olig2+/CC1+ cells within the demyelination lesion in healthy (CTL) or demyelinated control and mutant mice at 4, 8, 14 dpi. **(J-K)** Ki67+ immunolabeling shows the proliferation status of cells within the lesion 8dpi in control (J) and mutant (K) mouse. **(L)** Graph represents the cell proliferation (Ki67+ cells) in mutant relative to control mice at 4 and 8 dpi (n=9,12 control and n=8,16 mutant mice respectively). **(M-N)** Co-immunolabelling of Olig2 and Ki67 showing OPC proliferation in control (M) and mutant (N) mouse 8dpi. **(I)** Quantification of proliferating OPC (Ki67+/olig2+ cells) in lesion sites at 4 and 8 dpi (n=6,11 control and n=7,13 mutant mice respectively). Error bars represent S.E.M. *$p<0.05$,

***p<0.001, non-parametric Mann-Whitney test (independent two group comparisons). Scale bars: 50 µm in A, B, D, E and 10 µm in, G, H, J, K, M and N.

Figure 4- figure supplement 1. Ndst1 inactivation in oligodendrocyte lineage cells in *Olig2-Cre+/-; Ndst1 $^{Flox/Flox}$* mice. (A-B) Representative images of the lesion site (delineated by white dashed lines) in the corpus callosum of control **(A)** (n=2) and mutant **(B)** (n=2) mice at 8 dpi illustrating the enlargement of the lesion size in mutant mice compared to control mice. Olig2 (in red) is used to label oligodendrocyte lineage cells. In situ hybridization revealed a marked reduction in *Ndst1* expression surrounding the lesion site in mice with conditional inactivation in the oligodendroglial lineage cells (B, D, F) compared to control mice (A, C, E). C and D are high magnifications of the squares in A and B respectively. E and F are high magnifications of the squares in C and D respectively. Representative images of 10E4 immunostaining at the lesion site (delineated by white dashed lines. 8dpi) in the corpus callosum of control (G) and mutant (H) mice showing a strong reduction of heparan sulfate labeling in absence of Ndst1 in oligodendrocytes. CC, corpus callosum, V, ventricle, St, Striatum. Scale bars: 100 µm in A-; 20 µm in C-D. 30 µm in G-H

Figure 4 –figure supplement 2. Myelin content and glial density in adult unlesioned *Olig2-Cre+/-; Ndst1 $^{Flox/Flox}$* mice. (A-B) Representative images of the myelin content in the corpus callosum of control **(A)** and *Olig2-Cre; Ndst1 $^{Flox/Flox}$* **(B)** mice. **(C)** Quantitative analysis of the myelin content by double blind scoring of PLP staining in control (n=3) and mutant mice (n=3). Results are expressed in percentage of the control. **(D-E)** Astrocyte labeling by GFAP immunofluorescence in the corpus callosum of control **(D)** (n=2) and mutant (n=3) mouse brain **(E)**. **(G-H, J-K)** Phenotype of oligodendroglia in the corpus callosum of control **(G, J)** (n=5) and mutant **(H, K**) (n=5) mice by triple immunostaining for

Olig2/PDGFRα/CC1. **(F, I)** Quantification of mean cell density of astrocytes (GFAP+ cells) (n=2 and 3) **(F)** and oligodendroglia (Olig2+ cells) **(I)** in the corpus callosum of control and mutant mice (n=5 in each group). **(L)** Quantitative analysis of the percentage of Olig2+/CC1+ and Olig2+/PDGFRα+ in the corpus callosum of control and mutant mice (n=?). No significant difference was observed between the 2 groups using non-parametric Mann-Whitney test (independent two group comparisons). Error bars represent S.E.M. Scale bars: 10 µm.

Figure 5. Effect of *Ndst1* deletion on microglia/macrophage activation.

(A-B) CD68+/Ki67+ co-immunolabeling shows the proliferation status of activated microglia/macrophages. **(C)** Quantification of proliferating microglia/macrophages (Ki67+/CD68+ cells) in lesion sites at 4 and 8 dpi (n=3,7 control and n=3,7 mutant mice respectively). Iba1 (**D-E**) and CD68 immunolabeling **(F-G)** shows the increase in rhomboid-polarized microglia/macrophages in the demyelinated area of mutant mice at 8 dpi. **(H)** Quantification of the ratio of rhomboid/branched CD68+ cells in lesion sites at 4 and 8 dpi (n=3,4 control and n=3,6 mutant mice respectively) showing a switch of the microglia/macrophage polarization in favor of the rhomboid phenotype in mutant mice at 8 dpi. (**I-J**) Cox2 immunolabeling shows an increase in this M1 phenotype marker at 8dpi in mutant mice. (**K**) Quantification of Cox2+ cells in lesion sites at 8dpi (n=4 control and n=5 mutant mice). Error bars represent S.E.M. *$p \leq 0.05$, non-parametric Mann-Whitney test (independent two group comparisons). Scale bars: 50 µm in I-J and 10 µm in A-B, D-E, F-G.

Figure 6. AP-tagged Shh protein binds to HS concentrated around LPC-induced lesions in the corpus callosum. Representative images of adjacent serial coronal sections derived

from control mice 4 days after LPC injection and incubated with the fusion proteins AP-Shh-WT **(A-B')** or AP-Shh-CW in which the CW sequence responsible for HS binding is absent **(C-D)** (n=4)**.** The lesion site is delineated by dashed lines. Staining using B-gal is clearly visible around the lesion after AP-Shh incubation **(B-B'),** while no staining is observed when the AP-Shh-CW deleted protein is used **(D).** These data show that Shh is concentrated around the lesion and that this distribution depends on the integrity of the HS binding motif. **(E)** Quantification of Ptch1 expression at 8dpi in control and mutant mice reported in number of dots per cell (n=4 control and n=5 mutant mice). **(F-G)** Illustration of Ptch1 expression in peri-lesional areas in control (F) and mutant (G) mice after labeling as detected by RNAscope technology. CC, corpus callosum; Cx, cortex. Scale bars: 100µm in A-D. 10 µm in F and G.

Figure 7. NDST1 is highly expressed in MS tissue and NDST1+OLIG2+ cell density negatively correlates with lesion size. (A-B) Representative images of NDST1 staining in control **(A)** and MS **(B)** WM. **(C)** Quantification of NDST1 labeling shows a significant over-expression of NDST1 in MS lesions (n=9) compared to control tissue (n=4) (Kruskal-Wallis test, H=13.09, n=4,9,9, $p<0.01$, means plus standard deviation). The colors represent paired samples from the same patients. **(D-G)** Representative images of immunostaining against NDST1 successively co-labelled with OLIG2+ for oligodendroglia **(D)**, GFAP+ for astrocytes **(E)**, NEUN+ for neurons **(F)**, and IBA1+ for microglia/macrophages **(G)**. **(H)** Quantification of the proportions of different NDST1+ cell types in normal appearing WM and various MS lesions shows that NDST1 expressing cells are mainly oligodendroglia. **(I)** The proportion of OLIG2+ cells which is NDST1+ is significantly increased in active lesions compared to control (Kruskal-Wallis test, H=13.92, n=7,21,4,14,14 $p<0.05$). Overall, the majority of OLIG2+ cells are NDST1+ in MS lesions and NAWM while this is not true in control brain tissue. **(J)** The number of oligodendroglia expressing NDST1 is inversely correlated to lesion

size. **(K)** NDST1+ cell numbers positively correlate with the remyelination score assigned to each patient, summing all lesions within blocks from the same MS patients (see methods). NAWM, normal appearing white matter; RM, remyelinated lesion; A, active lesion; CA, chronic active lesion; CI, chronic inactive lesion. Scale bars represent 50 µm (A-B) or 10 µm (D-G).

Figure 7-figure supplement1. Comparisons of Ndst1 expression levels in control and MS brain tissue from all nuclei (A), or just oligodendroglia (B) showing a tendency to increased levels in MS samples. Data extracted from snRNA seq [37].

Figure 7-figure supplement2. NDST1 staining is specific and no lesion belt effect is observed in human brain. (A) Staining with NDST1 antibody in MS WM **(B)** There is no staining of MS WM with NDST1 antibody in in the presence of human recombinant NDST1. **(C)** LFB stain of MS tissue with the lesion delineated in red. **(D)** Representative NDST1+ staining in lesion (delineated with red line) shows uniform NDST1+ cell distribution. Scale bars: 100 µm.

	Patient	Sex	Age (years)	MS type	Disease duration (years)	Time to post mortem (h)	Number of lesions	Active	Chronic active	Chronic inactive	Remyeli-nating
MS	MS100	M	46	SP	8	7	6	0	0	4	2
	MS121	F	49	SP	14	24	2	1	0	1	0
	MS122	M	44	SP	10	16	2	1	1	0	0
	MS136	M	40	SP	9	10	9	1	0	3	5
	MS154	F	34	SP	21	12	4	2	0	1	1
	MS176	M	37	PP	27	12	7	0	0	2	5
	MS187	F	57	SP	27	13	4	0	0	0	4
	MS207	F	46	SP	25	10	8	0	3	3	2
	MS230	F	42	SP	19	31	4	2	0	0	2
Control	CO14	M	64	-	-	26	-	-	-	-	-
	CO25	M	35	-	-	22	-	-	-	-	-
	CO28	F	60	-	-	13	-	-	-	-	-
	CO39	M	82	-	-	21	-	-	-	-	-
Total							46	7	4	14	21

948 **Table 1: Classification and characteristic of human post-mortem samples.**

949

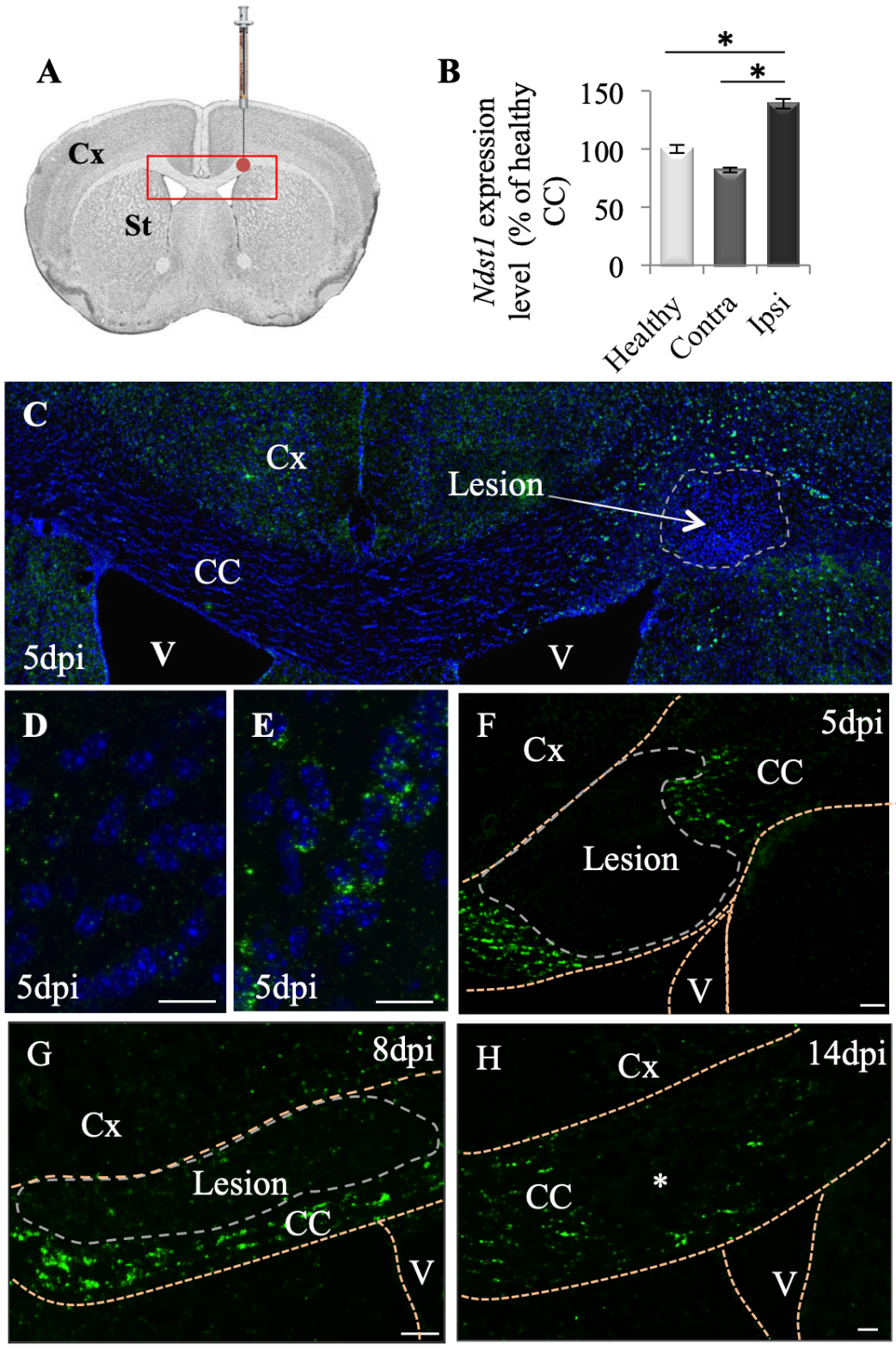
A
Cx
St
B
*
*
Ndst1 expression level (% of healthy CC)
150
100
50
0
H
Healthy
Contra
Ipsi
C
Cx
Lesion
CC
5dpi
V
V
D
5dpi
E
5dpi
F
5dpi
Cx
CC
Lesion
V
G
8dpi
Cx
Lesion
CC
V
H
Cx
14dpi
CC
*
V

Figure 1

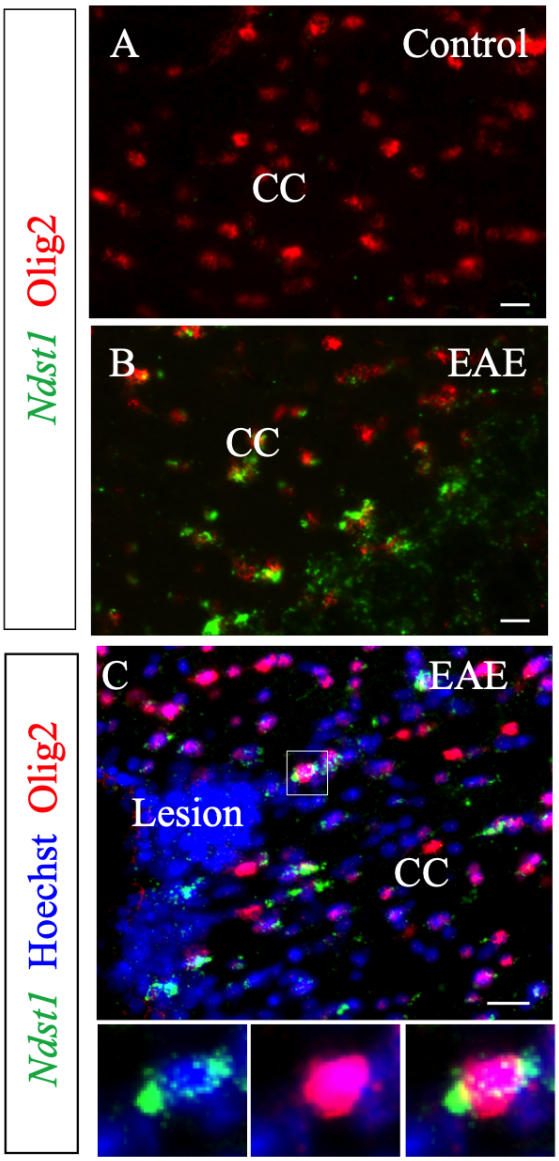

Figure1 supplement1

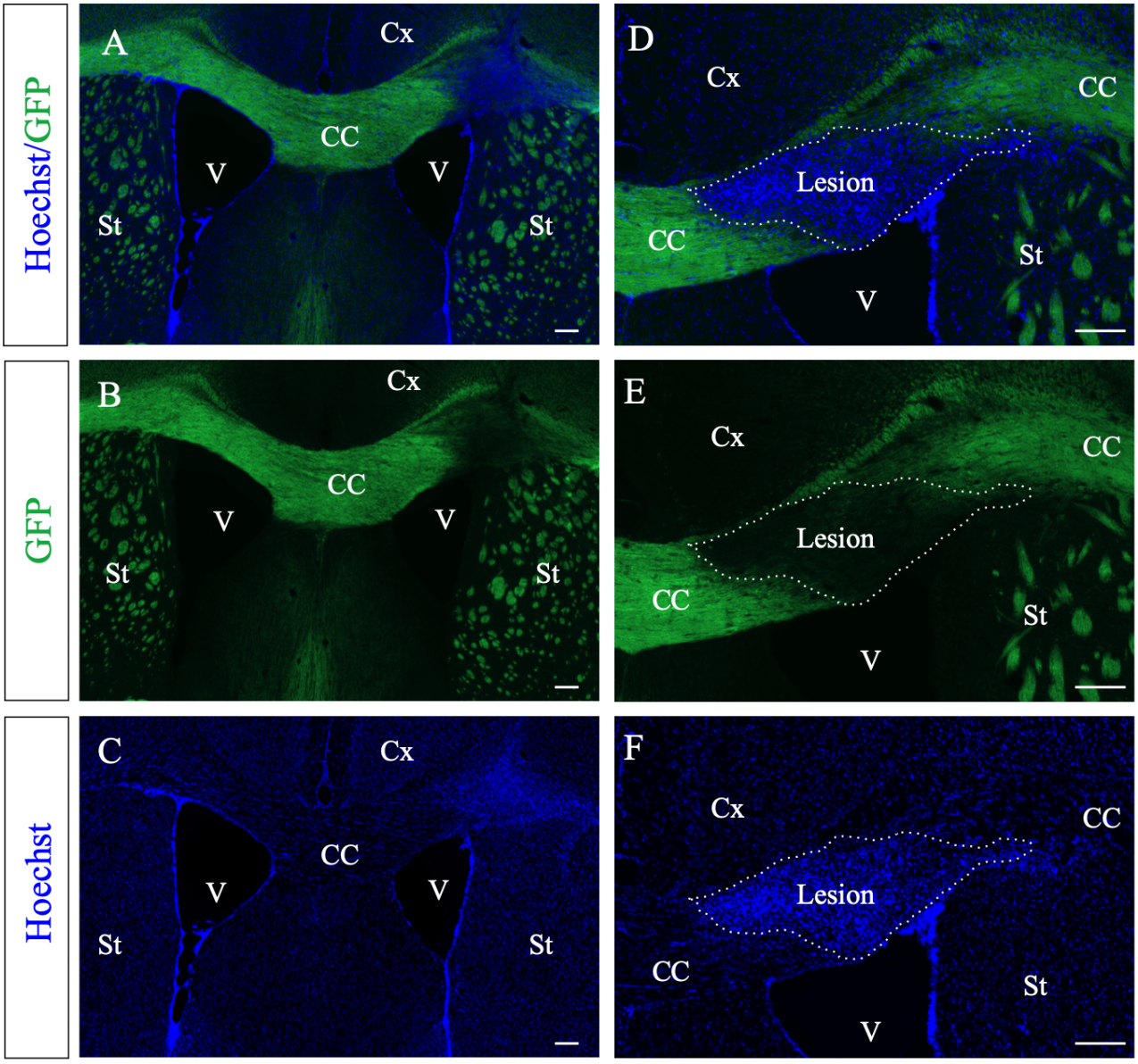

Figure1 Supplement2

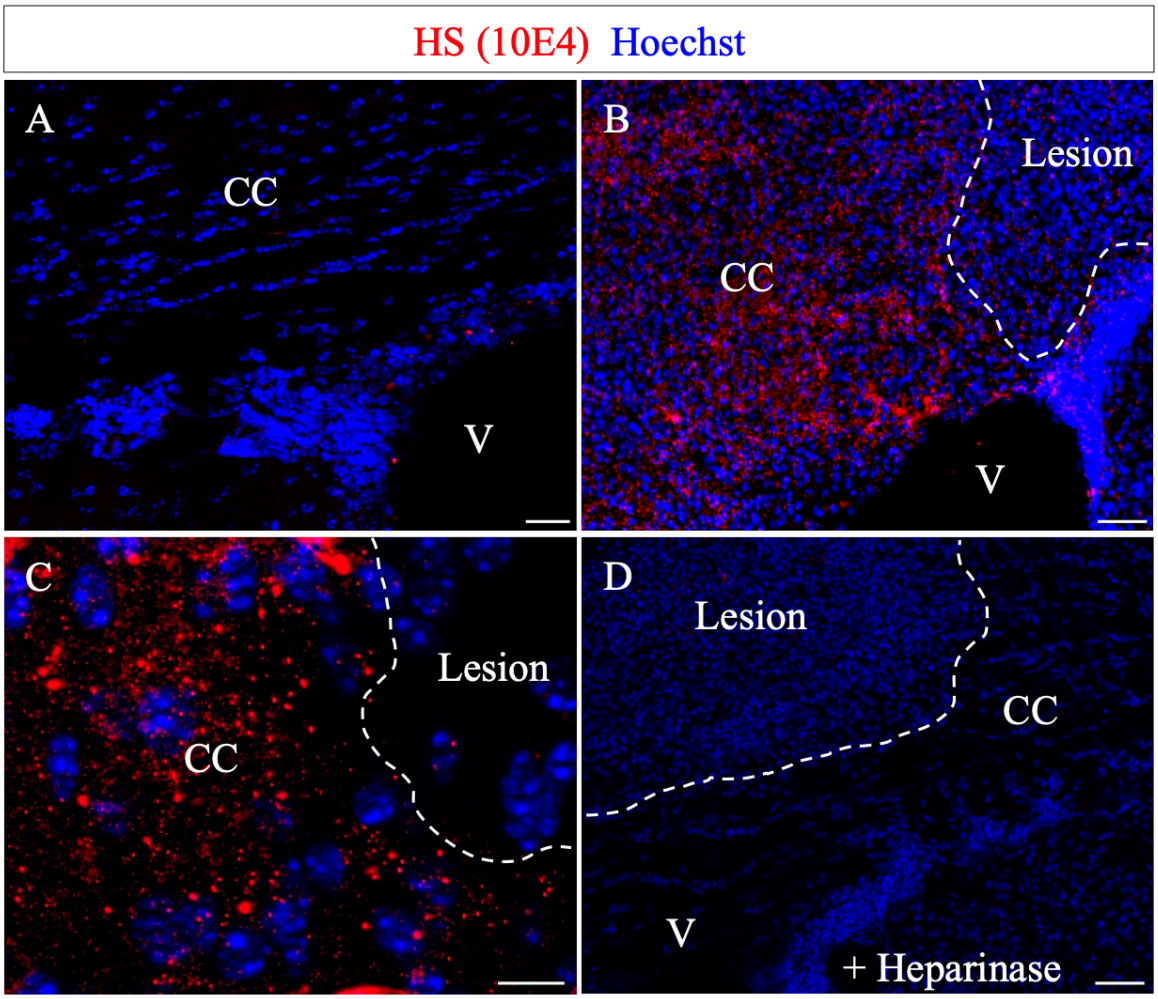
HS (10E4) Hoechst
A
CC
V
B
Lesion
CC
V
C
Lesion
CC
D
Lesion
CC
V
+ Heparinase

Figure 2

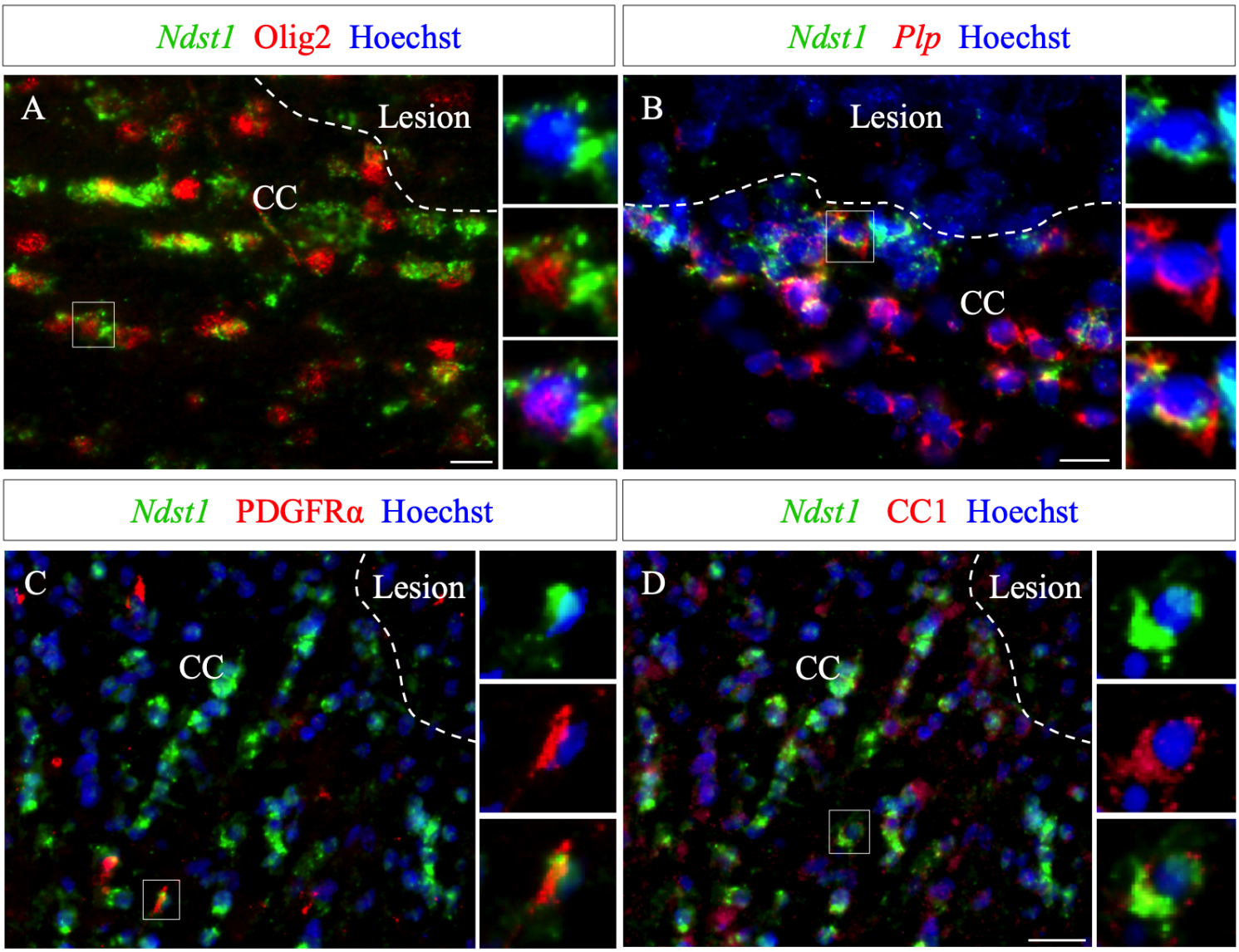
Ndst1 Olig2 Hoechst
A
Lesion
CC
Ndst1 Plp Hoechst
B
Lesion
CC
Ndst1 PDGFRα Hoechst
C
Lesion
CC
Ndst1 CC1 Hoechst
D
Lesion
CC

Figure 3

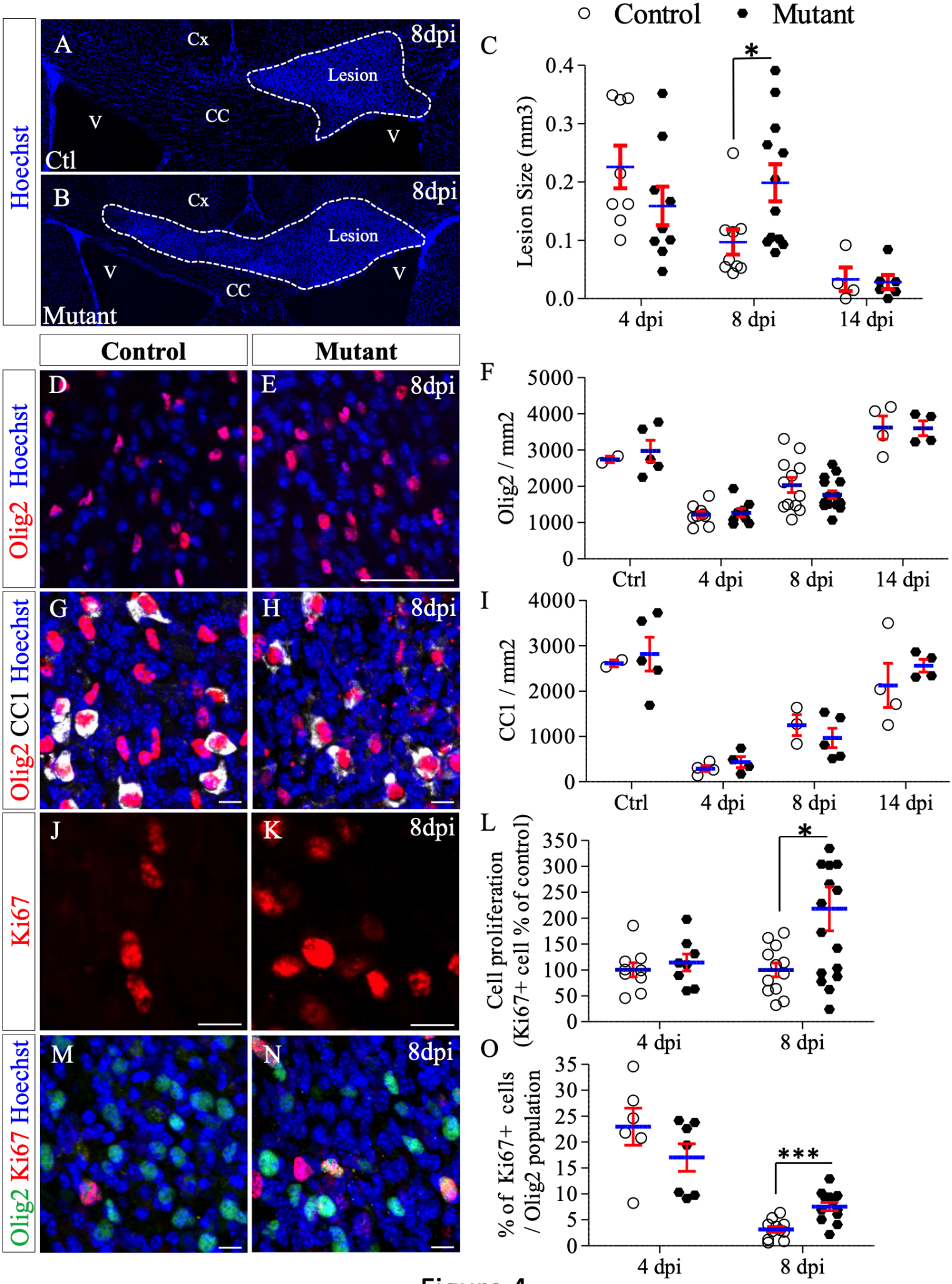
Hoechst
A
Cx
8dpi
Lesion
V
CC
V
Ctl
B
Cx
8dpi
Lesion
V
V
CC
Mutant
Control
Mutant
Olig2 Hoechst
D
E
8dpi
Olig2 CC1 Hoechst
G
H
8dpi
Ki67
J
K
8dpi
Olig2 Ki67 Hoechst
M
N
8dpi
C
Control
Mutant
Lesion Size (mm3)
0.4
0.3
0.2
0.1
0.0
*
4 dpi
8 dpi
14 dpi
F
Olig2 / mm2
5000
4000
3000
2000
1000
0
Ctrl
4 dpi
8 dpi
14 dpi
I
CC1 / mm2
4000
3000
2000
1000
0
Ctrl
4 dpi
8 dpi
14 dpi
L
Cell proliferation (Ki67+ cell % of control)
350
300
250
200
150
100
50
0
*
4 dpi
8 dpi
O
% of Ki67+ cells / Olig2 population
35
30
25
20
15
10
5
0
***
4 dpi
8 dpi

Figure 4

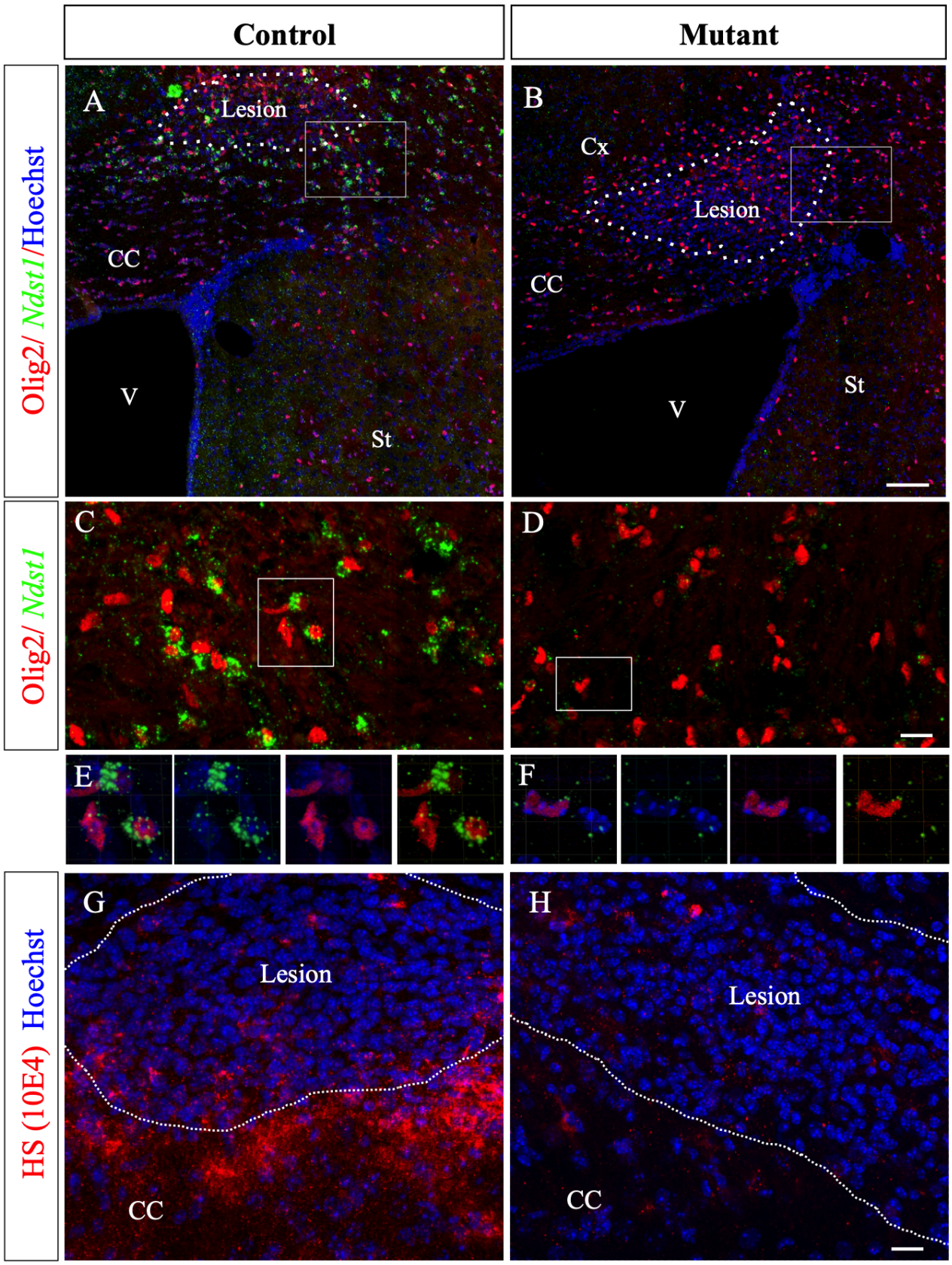

Figure 4 Supplement1

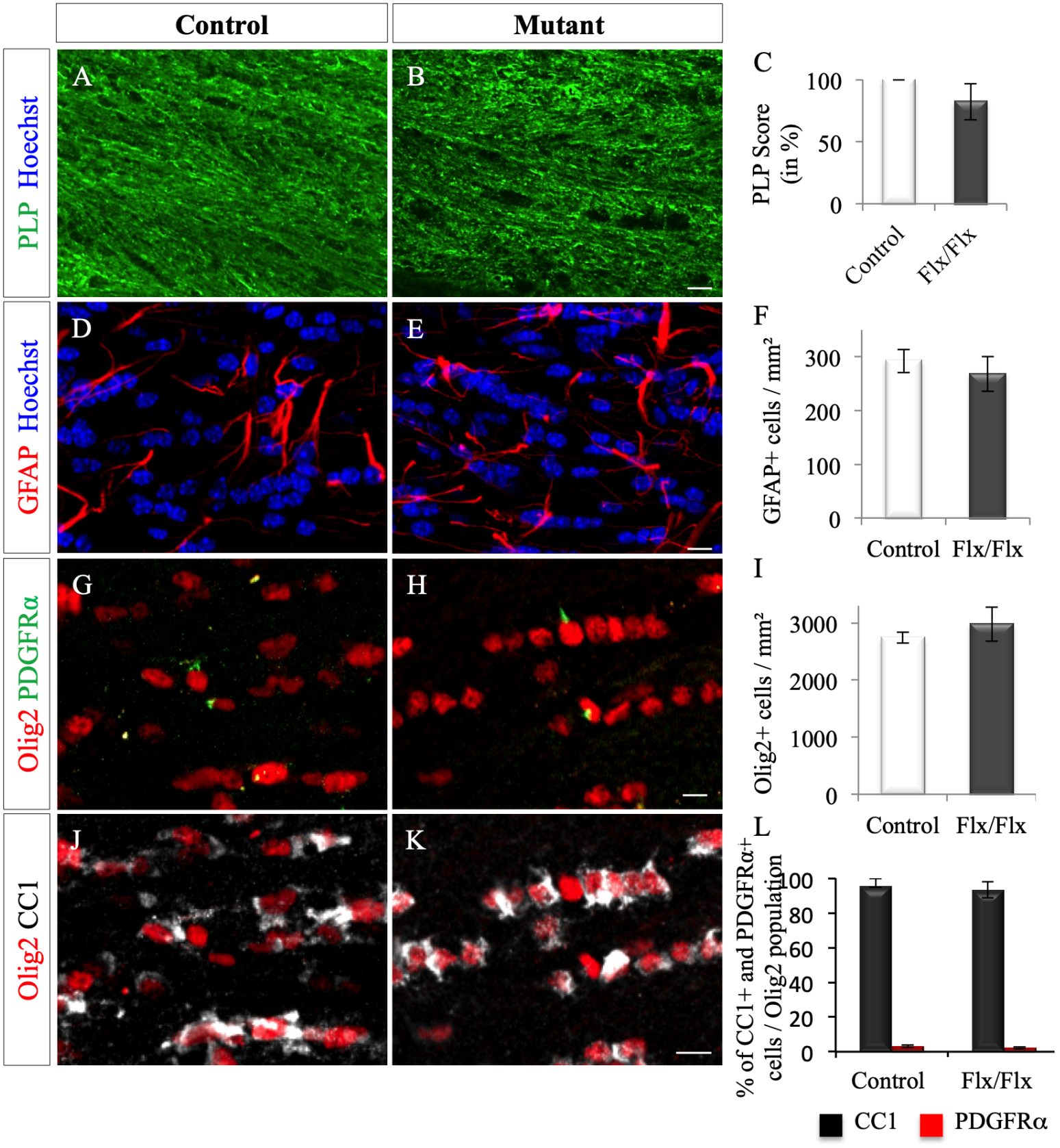

Figure 4 Supplement2

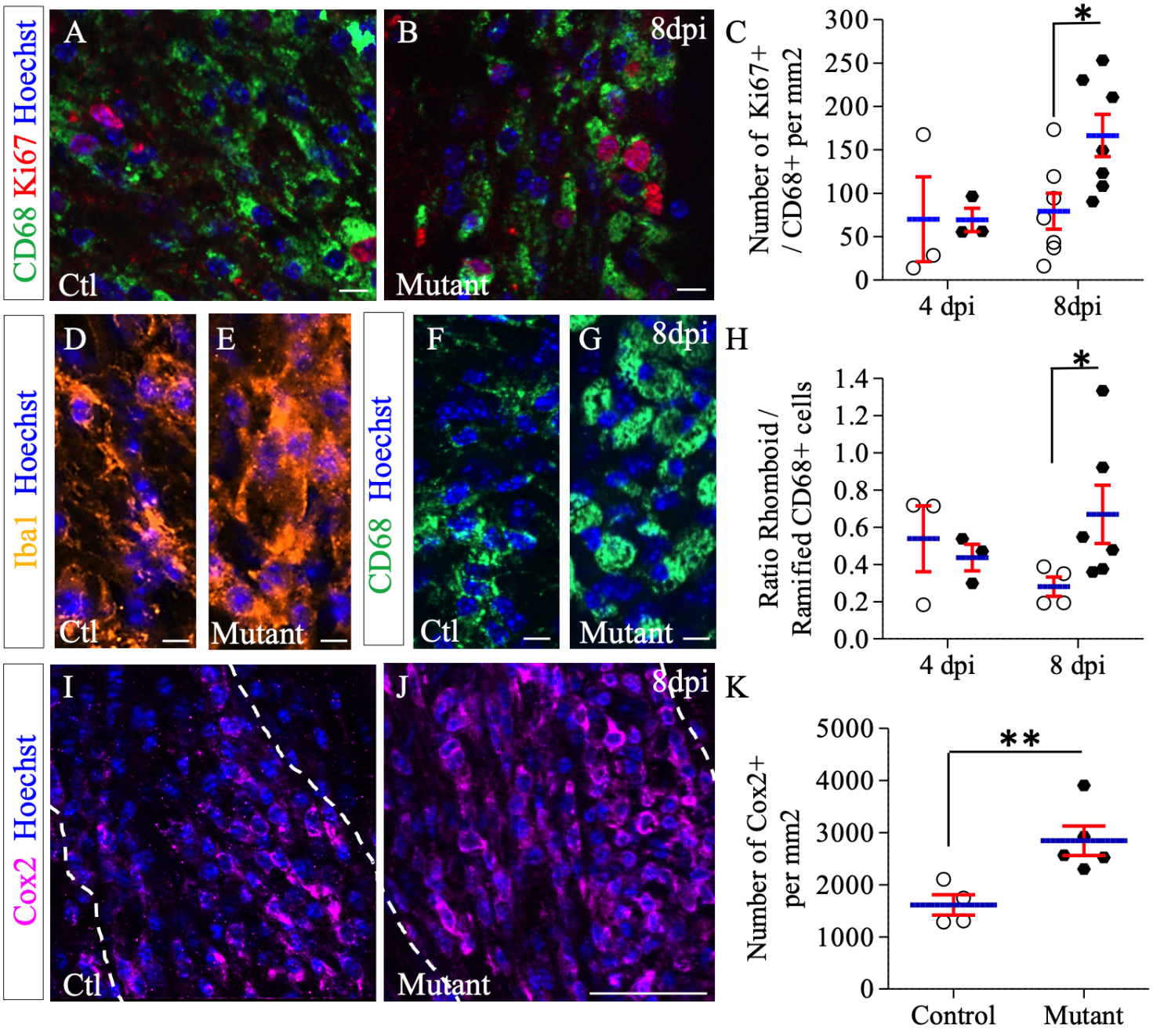
CD68 Ki67 Hoechst
A
Ctl
B
8dpi
Mutant
C
Number of Ki67+ / CD68+ per mm2
300
250
200
150
100
50
0
*
4 dpi
8dpi
Iba1 Hoechst
D
Ctl
E
Mutant
CD68 Hoechst
F
Ctl
G
8dpi
Mutant
H
Ratio Rhomboid / Ramified CD68+ cells
1.4
1.2
1.0
0.8
0.6
0.4
0.2
0.0
*
4 dpi
8 dpi
Cox2 Hoechst
I
Ctl
J
8dpi
Mutant
K
Number of Cox2+ per mm2
5000
4000
3000
2000
1000
0
**
Control
Mutant

Figure 5

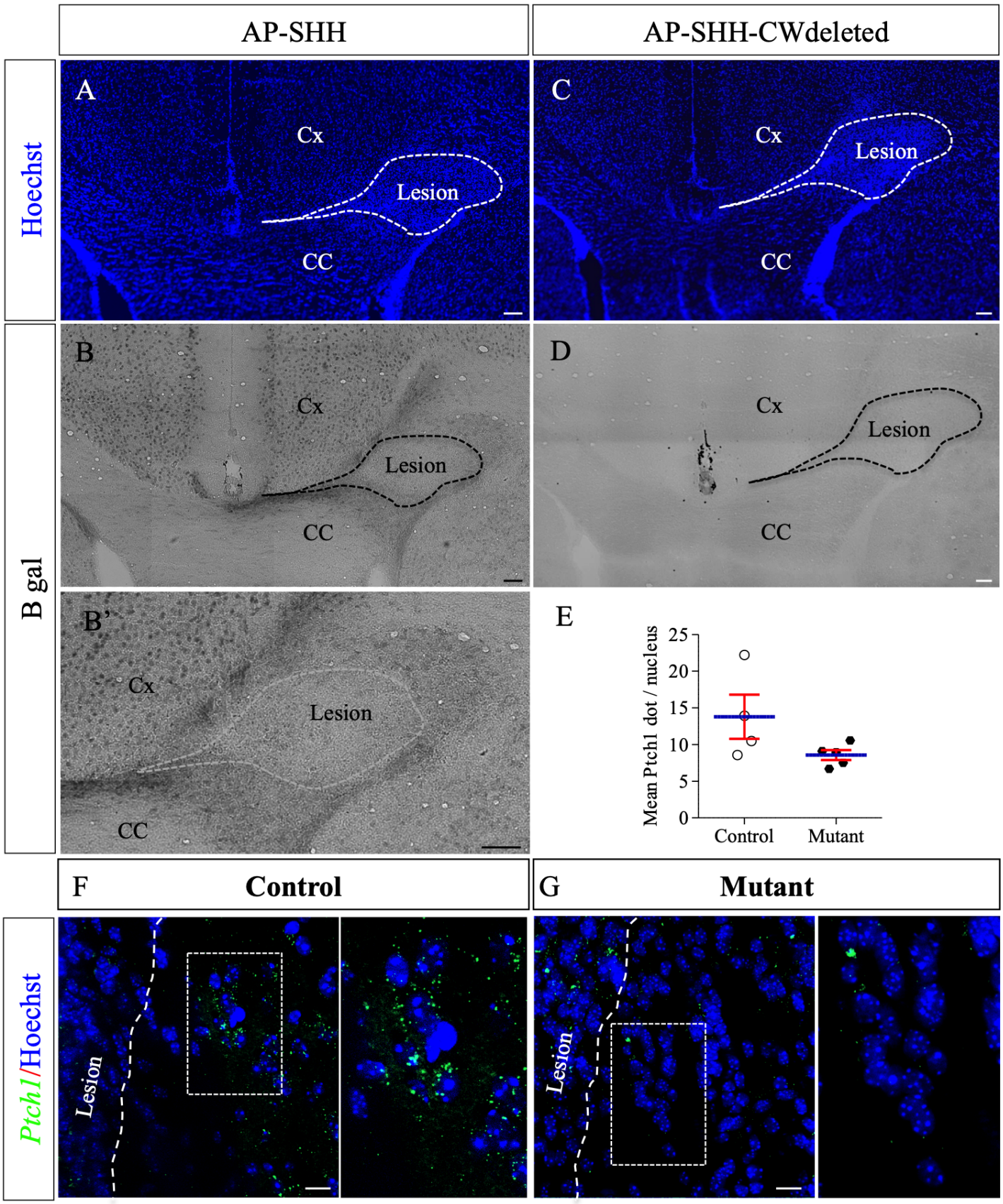
AP-SHH
AP-SHH-CWdeleted
Hoechst
B gal
A
C
B
D
B'
Cx
Lesion
CC
E
Mean Ptch1 dot / nucleus
25
20
15
10
5
0
Control
Mutant
F
Control
G
Mutant
Ptch1/Hoechst
Lesion

Figure 6

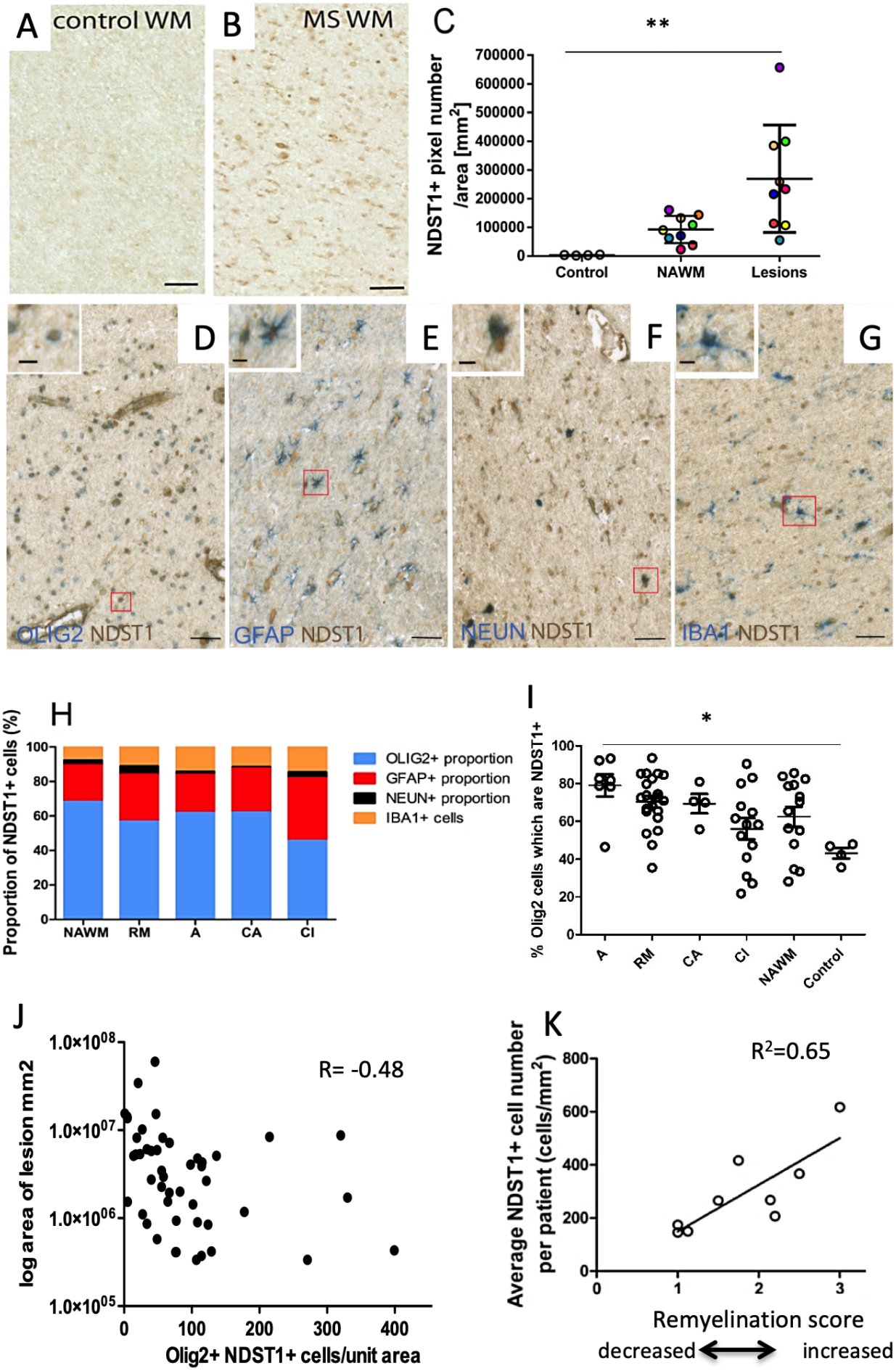
A
control WM
B
MS WM
C
**
NDST1+ pixel number /area [mm2]
700000
600000
500000
400000
300000
200000
100000
0
Control
NAWM
Lesions
D
E
F
G
OLIG2 NDST1
GFAP NDST1
NEUN NDST1
IBA1 NDST1
H
Proportion of NDST1+ cells (%)
100
80
60
40
20
0
NAWM
RM
A
CA
CI
OLIG2+ proportion
GFAP+ proportion
NEUN+ proportion
IBA1+ cells
I
*
% Olig2 cells which are NDST1+
100
80
60
40
20
0
A
RM
CA
CI
NAWM
Control
J
log area of lesion mm2
1.0×10^08
1.0×10^07
1.0×10^06
1.0×10^05
R= -0.48
0
100
200
300
400
Olig2+ NDST1+ cells/unit area
K
R2=0.65
Average NDST1+ cell number per patient (cells/mm2)
800
600
400
200
0
0
1
2
3
Remyelination score
decreased
increased

Figure 7

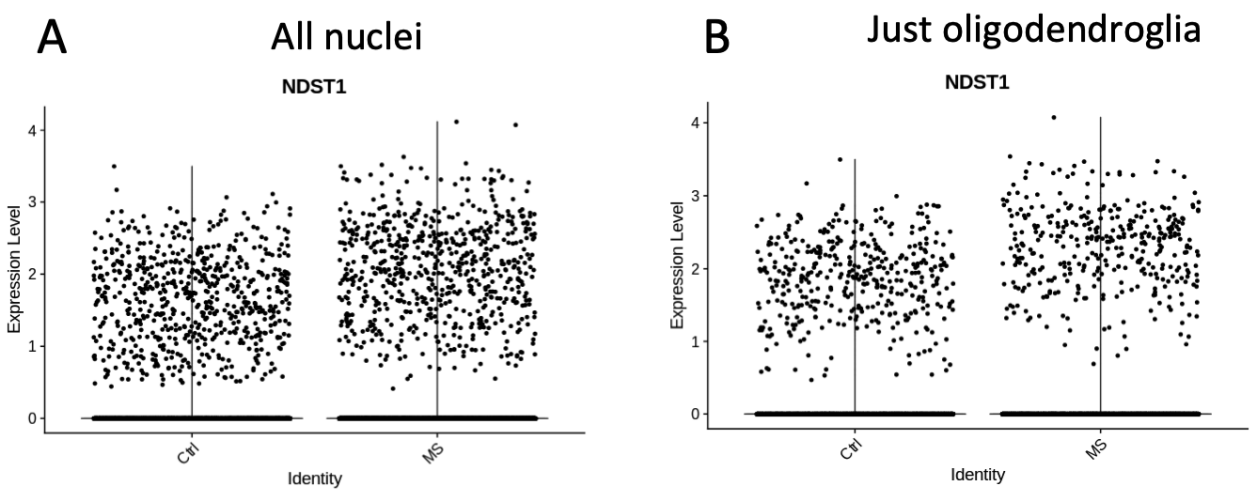

Figure7 Supplement1

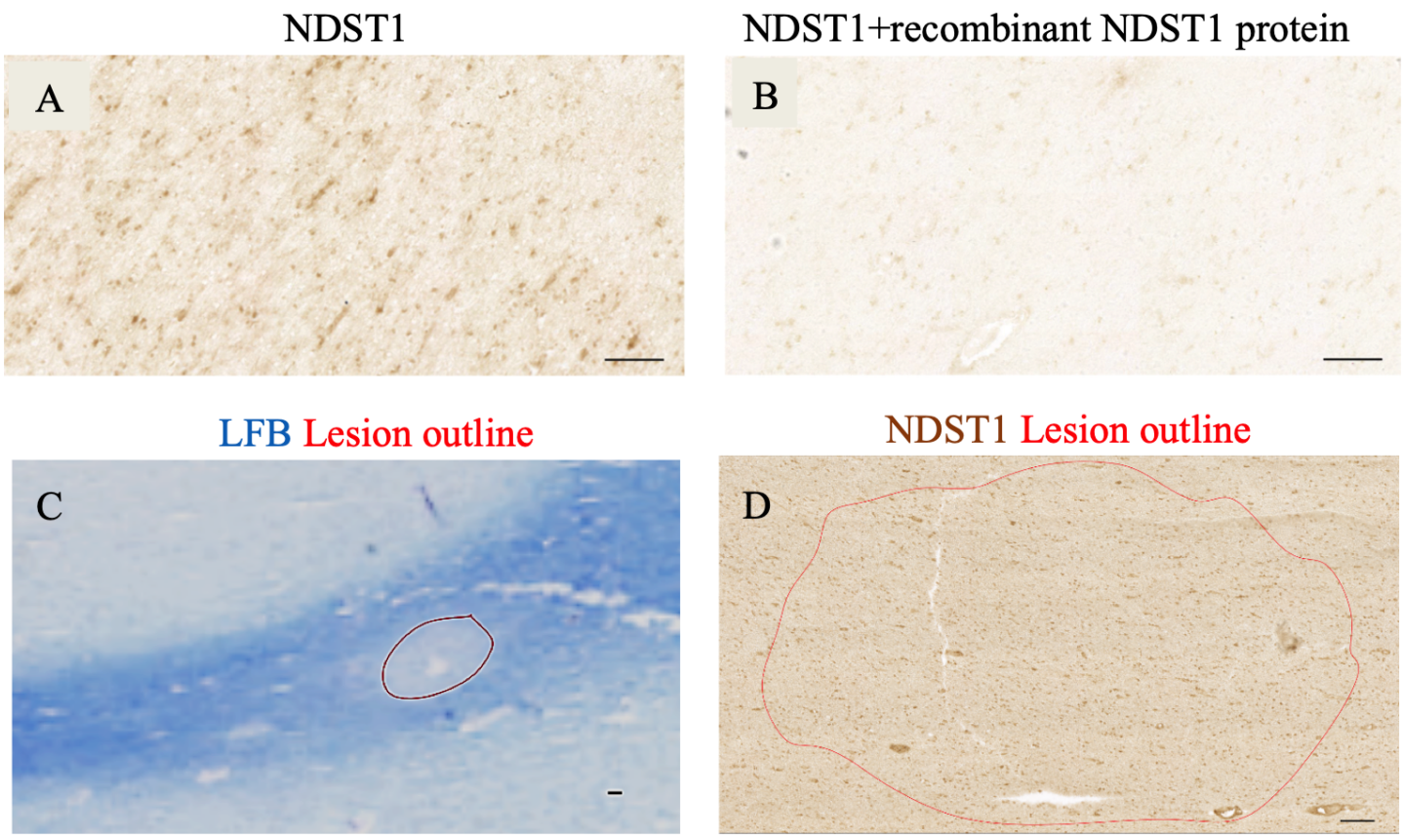

Figure 7 Supplement2